

Simple a posteriori error estimators in adaptive isogeometric analysis

Mukesh Kumar*, Trond Kvamsdal, Kjetil André Johannessen

Department of Mathematical Sciences, Norwegian University of Science and Technology, N-7491 Trondheim, Norway

Abstract

In this article we propose two simple a posteriori error estimators for solving second order elliptic problems using adaptive isogeometric analysis. The idea is based on a *Serendipity¹ pairing* of discrete approximation spaces $S_h^{p,k}(\mathcal{M})$ - $S_h^{p+1,k+1}(\mathcal{M})$, where the space $S_h^{p+1,k+1}(\mathcal{M})$ is considered as an enrichment of the original basis of $S_h^{p,k}(\mathcal{M})$ by means of the k -refinement, a typical unique feature available in isogeometric analysis. The space $S_h^{p+1,k+1}(\mathcal{M})$ is used to obtain a higher order accurate isogeometric finite element approximation and using this approximation we propose two simple a posteriori error estimators. The proposed a posteriori error based adaptive h -refinement methodology using LR B-splines are tested on classical elliptic benchmark problems. The numerical tests illustrate the optimal convergence rates obtained for the unknown, as well as the effectiveness of the proposed error estimators.

Keywords: Isogeometric analysis, B-splines, NURBS, LR B-splines, A posteriori error estimation, Local h -refinements, hpk -refinement, Adaptivity, Asymptotic exactness.

1. Introduction

1.1. Background

Isogeometric analysis (IGA) has been introduced in [24] as an innovative numerical methodology for the discretization of Partial Differential Equations (PDEs), the main idea was to improve the interoperability between CAD and PDE solvers, and to achieve this authors in [24] proposed to use CAD mathematical primitives, i.e. splines and NURBS, also to represent PDE unknowns. Isogeometric methods have been used and tested on a variety of problems of engineering interests, see [15, 24] and references therein. The development on mathematical front start with h -approximation properties of NURBS in [7], and further studies for hpk -refinements in [9] and for anisotropic approximation in [11]. The recently published article in Acta Numerica [10] provides a complete overview in this direction. Non-uniform rational B-splines (NURBS) are the dominant geometric representation format for CAD. The construction of NURBS are based on a tensor product structure and, as a consequence, knot insertion is a global operation. To remedy this a local refinement can be achieved by breaking the global tensor product structure of multivariate splines and NURBS. In the current literature there are three different ways to achieve local refinements: T-splines [37, 8, 17, 35], LR splines [16, 12, 27] and hierarchical splines [19, 23, 35, 29, 20, 40]. Recently, there has been much progress on the topic of the generalization of splines construction which allow for local refinement but an automatic reliable and efficient adaptive refinement routine is still one of the key issues in isogeometric analysis. To achieve a fully automatic refinement routine to solve PDEs problem in adaptive isogeometric analysis the *a posteriori error estimator* is required. This is the subject of current work.

The use of a posteriori error estimator in isogeometric analysis is still in its infancy. To the best of our knowledge only few work has been done in this direction, see [13, 17, 28, 36, 38, 40, 41, 42, 43]. The authors in [17] used the idea

¹According to Wikipedia: *Serendipity* means a “fortunate happenstance” or “pleasant surprise”. It was coined by Horace Walpole in 1754. One aspect of Walpole’s original definition of Serendipity is the need for an individual to be “sagacious” enough to link together apparently innocuous facts in order to come to a valuable conclusion. We feel that this applies for the present discovery, but it is of course up to the readers to judge.

*Corresponding author

Email addresses: Mukesh.Kumar@math.ntnu.no (Mukesh Kumar), Trond.Kvamsdal@math.ntnu.no (Trond Kvamsdal), Kjetil.Andre.Johannessen@math.ntnu.no (Kjetil André Johannessen)

of hierarchical bases with bubble functions approach of Bank and Smith [5] to design a posteriori error estimator for T-splines, which was also considered in [13, 40]. Another simple idea of explicit residual based error estimator has been explored in [14, 26, 38, 41, 42, 43]. They require the computation of constants in Clement-type interpolation operators. Such constant are mesh (element) dependent and often incomputable for general element shape. A global constant can overestimate the local constants, and thus the exact error. Recently, a functional-type a posteriori error estimate for isogeometric discretization is presented in [28]. These type of error estimate, which was originally introduced in [32, 33] on functional grounds (including integral identity and functional analysis arguments) are applicable for any conforming and non-conforming discretizations and known to provide a guaranteed and computable error bounds. But the hindrance in their popularity is due to high cost of computations which are based on solving a global minimization problem (Majorant minimization problem) in $H(\text{div})$ spaces. In [28], authors made an attempt to reduce the cost of computations for tensorial spline spaces but the same idea of cost reduction need further study in adaptive isogeometric analysis. To the best of authors knowledge, in the above mentioned work on the use of a posteriori error estimators in isogeometric analysis the role of error estimator has been limited to either just as an indicator to perform adaptive refinement steps or the error estimation computation is given on tensorial mesh. A complete study about the performance of error estimators in adaptive analysis which makes them a suitable candidate for both the error estimation and adaptivity has not been considered so far. Recently, the present authors have presented a recovery based approach for establishing efficient error estimator in adaptive isogeometric analysis [30]. The approach is based on Superconvergent Patch Recovery (SPR) procedure (original idea of Zienkiewicz-Zhu [44]) that is enhanced to be applicable within isogeometric analysis. The enhancement includes procedure for numerically computing the location of true superconvergent points. Extensive numerical tests have been performed on elliptic benchmark problems to show the efficiency of the develop SPR approach.

In this article we present another possibility to design a posteriori error estimators in adaptive isogeometric analysis. The employed technique is based on solving the original problem with two discretization schemes of different accuracy and using the difference in the approximations as an estimate of the error, see [21] and Chapter 5 in [2]. Consider the elliptic model problems of Section 5.1 and suppose that the numerical approximation u_h in Finite Element (FE) subspace V_h is known. Then in classical Finite Element Methods (FEM), the enhanced space V_h^* may, for example, be constructed by either global h -refinement or p -refinement of the mesh use to construct the original FE subspace V_h , see [2, 4, 5, 6, 18]. Suppose $u_h^* \in V_h^*$ is the another FE approximation to the original problem then after using the triangle inequality on the energy error (the energy norm is induced by the bilinear form of the underlying self adjoint elliptic problem as given by Eq. (35)) can be written as

$$\|e\|_E = \|u - u_h\|_E \leq \underbrace{\|u_h^* - u_h\|_E}_{\text{Computable}} + \underbrace{\|u - u_h^*\|_E}_{\text{Non-Computable}} . \quad (1)$$

If we assume that the approximation $u_h^* \in V_h^*$ is superior to the original approximation u_h , then

$$\|e\|_E \approx \|u_h^* - u_h\|_E = \eta_h^* \quad (\text{Computable error estimate}). \quad (2)$$

The enhanced subspace V_h^* based on global h - or p -refinement of the element of original subspace V_h clearly satisfies $V_h \subset V_h^*$. From a priori error estimation results in classical FEM, for a sufficiently smooth solution u it has been observed that $\|u - u_h^*\|_E \leq C_\theta \|u - u_h\|_E$, where $C_\theta \in [0, 1)$ for h -refined subspace V_h^* and $C_\theta = O(h)$ for p -refined subspace V_h^* . It is seen in literature that the adaptive simulations based on the error estimator η_h^* also provide the asymptotic exactness result on refined meshes, see [2, 4, 5, 6, 18]. The attractiveness of such ideas stems from their applicability to quite general classes of problems combined with simplicity and ease of implementation.

In isogeometric analysis, there are several possibilities to obtain a higher order approximation u_h^* from the space V_h^* . In comparison to the h - and p -refinement available in classical FEA, isogeometric analysis offers a new possibility of k -refinement in which the global continuity and degree are increased together. Suppose $S_h^{p,k}(\mathcal{M})$ is the given isogeometric FE subspace of degree p , continuity k with size of elements h on the mesh \mathcal{M} . Then the following

approximation spaces can be obtained under these operations:

$$S_h^{p,k}(\mathcal{M}) \xrightarrow{\text{h-refinement}} S_{h/2}^{p,k}(\bar{\mathcal{M}}) \quad (3)$$

$$S_h^{p,k}(\mathcal{M}) \xrightarrow{\text{p-refinement}} S_h^{p+1,k}(\mathcal{M}) \quad (4)$$

$$S_h^{p,k}(\mathcal{M}) \xrightarrow{\text{k-refinement}} S_h^{p+1,k+1}(\mathcal{M}) \quad (5)$$

where $S_{h/2}^{p,k}(\bar{\mathcal{M}})$, $S_h^{p+1,k}(\mathcal{M})$, and $S_h^{p+1,k+1}(\mathcal{M})$ represents the isogeometric FE subspaces obtained after performing the uniform h -, p -, and k -refinement on the subspace $S_h^{p,k}(\mathcal{M})$, respectively. It should be noted that for p - and k -refinement the integration mesh \mathcal{M} will remain the same, whereas the continuity of the basis functions across the element boundaries will increase by one for the case with k -refinement. For the case of h -refinement we obtain a new mesh $\bar{\mathcal{M}}$ that is a uniform h -refinement of the original mesh \mathcal{M} , i.e. all the elements are halved.

1.2. Outline of the article

In Section 2 we first discuss the general behavior of some different approaches available in isogeometric analysis to refine a given discrete approximation space V_h into V_h^* in order to obtain a more accurate approximation u_h^* compared to u_h . Based on our arguments given in this section we advocate the use of enrichment of the original basis of $S_h^{p,k}(\mathcal{M})$ by means of k -refinement to construct the approximation space V_h^* . The definitions of B-splines, NURBS and LR B-splines which is necessary to build an approximation space in isogeometric analysis is briefly introduced in Section 3. For adaptive isogeometric analysis, we present in Section 4 the construction of discrete pair of isogeometric k -refined approximation spaces $S_h^{p,k}(\mathcal{M})$ - $S_h^{p+1,k+1}(\mathcal{M})$ using LR B-splines technology of [27]. In case of adaptive LR meshes, we observe that

$$\dim S_h^{p+1,k+1}(\mathcal{M}) \approx \dim S_h^{p,k}(\mathcal{M}) \quad (6)$$

i.e. the dimension of the k -refined space is approximately equal to the unrefined space. Furthermore, the integration LR meshes are the same for this two spaces at each adaptive refinement level. Using the *serendipity pairing* of discrete approximation spaces $S_h^{p,k}(\mathcal{M})$ and $S_h^{p+1,k+1}(\mathcal{M})$ we propose two simple a posteriori error estimators η_h^* and η_h^{RES} for solving second order elliptic problems using adaptive isogeometric analysis in Section 5. The first error estimator η_h^* represents the computable part of Eq. (1) while the second error estimator η_h^{RES} in addition try to estimate the non-computable part of the error from (1). In Section 6 we investigate the numerical performance of the two a posteriori error estimators on a smooth and non-smooth elliptic benchmark problems. We present results obtained regarding the convergence rate for the unknown u^h as well as the effectivity index of the different error estimators. Furthermore, we briefly report results obtained by an even more cost efficient approach where we consider a coarser mesh but higher order k -refined spaces $S_{mh}^{p+m,k+m}$, $m = 1, 2, 4$. We end this article in Section 7 with some concluding remarks and future prospectives.

2. Enrichment approaches to obtain a more accurate approximation

In this section we present the general behavior of different approaches to obtain a more accurate approximation u_h^* compared to u_h in isogeometric analysis by means of enrichment of the original basis of $S_h^{p,k}(\mathcal{M})$. We mainly focus on the dimension ratio, accuracy per degree of freedom, and cost involved in obtaining a more accurate approximation. We fix the notation by considering $V_h := S_h^{p,k}(\mathcal{M})$ and V_h^* the respective approximation spaces obtained from the h -, p - and k -refinement of V_h .

2.1. Dimension ratio between $S_h^{p,k}(\mathcal{M})$ and its h -, p -, and k -refinement counterparts

On tensorial meshes in the parametric domain $\Omega := [0, 1]^2$, suppose $\dim S_h^{p,k}(\mathcal{M}) = n_{dim} \times n_{dim}$ then its uniformly refined counterparts will have the following dimensions:

$$\dim S_{h/2}^{p,k}(\bar{\mathcal{M}}) = (2n_{dim} - k - 1) \times (2n_{dim} - k - 1), \quad (7)$$

$$\dim S_h^{p+1,k}(\mathcal{M}) = (n_{dim} + \frac{1}{h}) \times (n_{dim} + \frac{1}{h}), \quad (8)$$

$$\dim S_h^{p+1,k+1}(\mathcal{M}) = (n_{dim} + 1) \times (n_{dim} + 1). \quad (9)$$

For a large systems, i.e. $\frac{1}{h} \gg p > k$ the relation between the dimension of original spline space $\mathcal{S}_h^{p,k}(\mathcal{M})$ and its uniformly refined counterparts in 1D, 2D and 3D are also presented in Table 1. It can be observed from Table 1 that the dimension of $\mathcal{S}_{h/2}^{p,k}(\bar{\mathcal{M}})$ and $\mathcal{S}_h^{p+1,k}(\mathcal{M})$ are four times the dimension of $\mathcal{S}_h^{p,k}(\mathcal{M})$, while the k -refined space $\mathcal{S}_h^{p+1,k+1}(\mathcal{M})$ has almost equal dimension as the space $\mathcal{S}_h^{p,k}(\mathcal{M})$.

Table 1: Dimension ratio between $\mathcal{S}_h^{p,k}(\mathcal{M})$ and its h -, p -, and k -refined counterparts.

Degree	Continuity	h -refinement			p -refinement			k -refinement		
		$r_h = \frac{\dim \mathcal{S}_{h/2}^{p,k}}{\dim \mathcal{S}_h^{p,k}}$	$r_p = \frac{\dim \mathcal{S}_h^{p+1,k}}{\dim \mathcal{S}_h^{p,k}}$	$r_k = \frac{\dim \mathcal{S}_h^{p+1,k+1}}{\dim \mathcal{S}_h^{p,k}}$	1D	2D	3D	1D	2D	3D
4	3	2	4	8	2	4	8	1	1	1
	2	2	4	8	1.5	2.25	3.38	1	1	1
	1	2	4	8	1.33	1.77	2.35	1	1	1
	0	2	4	8	1.25	1.56	1.95	1	1	1

2.2. Accuracy per degree of freedom

On the tensorial meshes the h - and p -refined spaces of $\mathcal{S}_h^{p,k}$ clearly satisfies $\mathcal{S}_h^{p,k} \subset \mathcal{S}_{h/2}^{p,k}$ and $\mathcal{S}_h^{p,k} \subset \mathcal{S}_h^{p+1,k}$, respectively. This property makes these spaces a natural candidate to obtain more accurate approximations. In Figure 1, we compare the energy norm errors obtained by solving the two dimensional self-adjoint elliptic problem denoted *Sinus problem* given in Example 1 of Section 6 using different enhanced approximation spaces for $V_h := \mathcal{S}_h^{p,k}$ of degree $p = 2$. The comparison for the energy norm errors given in Figure 1 shows that an increase in approximation accuracy is achieved for h - and p -refined spaces, but with a significant increase in number of degrees of freedom. In contrary, for the k -refined space we have that $\mathcal{S}_h^{p,k} \not\supset \mathcal{S}_h^{p+1,k+1}$ and $\mathcal{S}_h^{p,k} \not\subset \mathcal{S}_h^{p+1,k+1}$. However, an increase in approximation order is still achieved, but now with minimal increase in number of degrees of freedom. Here we have considered an example of the elliptic problem with smooth solution, whereas we in Section 6 show results obtained for a non-smooth benchmark problem.

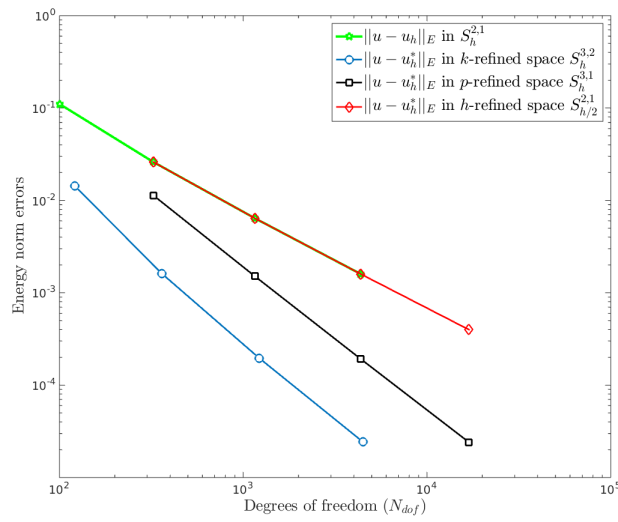


Figure 1: **Sinus problem:** Energy errors with uniform h -refinements of $\mathcal{S}_h^{2,1}$ and its h -, p - and k -refined spaces.

2.3. Computational cost comparison

Another important aspect to be taken into account before choosing enrichment strategy is the computational costs involved. We have therefore investigated the computational effort used for the h -, p - and k -refinement com-

pared to the computational cost for finding the original solution u^h . We have chosen to split the the total costs into two categories: (i) Assembly of the linear equation system (including formation of the element matrices) and (ii) Solving the linear equation system. We have again addressed the smooth problem given in Example 1 of Section 6 and Table 2 shows the obtained cost ratios for each level in a sequence of uniform mesh refinement. We see from the columns presenting the assembly cost ratio and total time ratio that the approximation u_h^* obtained from the h -refined approximation space is four times more costly than the original approximation u_h itself. While the total cost involved for the p - and k -refined approximations are almost equal and approximately twice to the cost of original approximation u_h . However, notice that the solving time ratio for p -refinement is more than four times compared to the solving time for the the original approximation u_h , whereas for k -refinement the ratio is slightly above one.

From the results of Table 2 it is clear that for all cases the assembly time are greater than the solving time. So even though the k -refined space has less number of degrees of freedom than the p -refined space the total solution time is similar as they have the same number of elements which is of greatest importance for the assembly time. The high cost related to assembly is a well known drawback for isogeometric analysis compared to classical low order Lagrange finite elements. This has sparked a renewed research interest into development of more efficient numerical quadrature for splines. Some developments in constructing selective and reduced integration rules for isogeometric analysis based on B-splines/NURBS elements are given in [1],[3],[22], [34], [25]. A more recent variationally consistent domain integration approach of [22] allows a significant reduction in the number of quadrature points while maintaining the stability, accuracy, and optimal convergence properties as high order quadrature rules. For example, in case of quadratic C^1 and cubic C^2 splines one Gauss points per internal element and p points per element where repeated knot exists, has been proposed. The present authors expect that *in near future* (after some more research) these kind of approaches will become well proven methods for isogeometric analysis such that the assembly cost will be less than the corresponding solving time for realistic scientific and industrial applications. Hence, the k -refinement will eventually be less costly than the p -refinement.

The above arguments about the dimension ratio, accuracy per degree of freedom, and computational cost involved in obtaining a more accurate approximation clearly show that the p -refined space $\mathcal{S}_h^{p+1,k}$ and k -refined space $\mathcal{S}_h^{p+1,k+1}$ are a preferred choice over the h -refined space $\mathcal{S}_{h/2}^{p,k}$. Furthermore, notice that the p - and k -refinement achieve a *higher order* approximation, whereas the h -refinement does not (h -refinement results in more accurate solution but with same convergence order, see Figure 1).

The p -refined space is of significant larger dimension than the original space $\mathcal{S}_h^{p,k}$ which implies a larger data set to handle by the computer and increased solving time (as shown in Table 2). On the other hand for globally tensorial meshes an enhanced higher order approximation is obtained with the *embedding* property $\mathcal{S}_h^{p,k} \subset \mathcal{S}_h^{p+1,k}$. However, in an adaptive setting one needs to design a local refinement algorithm which satisfies this property at each level of the adaptive process, and that is in general non-trivial. To the contrary, the k -refined spaces do not satisfy the embedding property, i.e. $\mathcal{S}_h^{p,k} \not\supset \mathcal{S}_h^{p+1,k+1}$ and $\mathcal{S}_h^{p,k} \not\subset \mathcal{S}_h^{p+1,k+1}$, but an increase in approximation order is still achieved and now with minimal increase in the number of degrees of freedom. Furthermore, k -refinement is easier to realize in an adaptive setting since we don't have the “embedding property to fulfill”.

Based on the fact that the selective and reduced integration rules will be available in near future for isogeometric analysis we advocate to use the k -refined approximation spaces in obtaining higher order approximation u_h^* . We will herein use u_h^* (obtained by means of k -refinement) to design some a posteriori error estimators for solving elliptic problems in adaptive isogeometric analysis. Although the present authors prefer to use the same integration meshes for V_h and V_h^* in adaptive analysis, we also propose in Section 6 some cost efficient k -refinement approaches where we use higher order but coarse grid to obtain spaces $V_{mh}^* := \mathcal{S}_{mh}^{p+m,k+m}$, $m = 1, 2, 4$. This unique setting of involving higher order combined with coarse meshes k -refined spaces can reduce the computational cost ratio compared to solving u^h to less than 0.5.

Table 2: **Sinus problem**: Degrees of freedoms and timings, Case: $V_h = \mathcal{S}_h^{2,1}(\mathcal{M})$ with different spaces V_h^* .

k-refinement: $V_h = \mathcal{S}_h^{2,1}(\mathcal{M})$ and $V_h^* = \mathcal{S}_h^{3,2}(\mathcal{M})$						
Mesh size	Degrees of freedom			Assembling time	Solving time	Total
	$N_{dof} = \dim(V_h)$	$N_{dof}^* = \dim(V_h^*)$	$\frac{N_{dof}^*}{N_{dof}}$	$\frac{FE(u_h^*)}{FE(u_h)}$	$\frac{FE(u_h^*)}{FE(u_h)}$	$\frac{FE(u_h^*)}{FE(u_h)}$
4 × 4	36	49	1.36	1.12	1.07	1.12
8 × 8	100	121	1.21	1.36	1.38	1.36
16 × 16	324	361	1.11	1.51	1.98	1.52
32 × 32	1156	1225	1.06	1.61	2.03	1.62
64 × 64	4356	4489	1.03	1.66	2.00	1.66
128 × 128	16900	17161	1.01	1.70	2.11	1.70

h-refinement: $V_h = \mathcal{S}_h^{2,1}(\mathcal{M})$ and $V_h^* = \mathcal{S}_{h/2}^{2,1}(\tilde{\mathcal{M}})$						
Mesh size	Degrees of freedom			Assembling time	Solving time	Total
	$N_{dof} = \dim(V_h)$	$N_{dof}^* = \dim(V_h^*)$	$\frac{N_{dof}^*}{N_{dof}}$	$\frac{FE(u_h^*)}{FE(u_h)}$	$\frac{FE(u_h^*)}{FE(u_h)}$	$\frac{FE(u_h^*)}{FE(u_h)}$
4 × 4	36	100	2.78	0.68	0.70	0.68
8 × 8	100	324	3.24	2.89	16.61	2.91
16 × 16	324	1156	3.57	3.26	5.91	3.28
32 × 32	1156	4356	3.77	3.61	4.92	3.62
64 × 64	4356	16900	3.88	3.77	4.70	3.78
128 × 128	16900	66564	3.93	3.91	4.88	3.93

p-refinement: $V_h = \mathcal{S}_h^{2,1}(\mathcal{M})$ and $V_h^* = \mathcal{S}_h^{3,1}(\mathcal{M})$						
Mesh size	Degrees of freedom			Assembling time	Solving time	Total
	$N_{dof} = \dim(V_h)$	$N_{dof}^* = \dim(V_h^*)$	$\frac{N_{dof}^*}{N_{dof}}$	$\frac{FE(u_h^*)}{FE(u_h)}$	$\frac{FE(u_h^*)}{FE(u_h)}$	$\frac{FE(u_h^*)}{FE(u_h)}$
4 × 4	36	100	2.78	1.01	1.44	1.01
8 × 8	100	324	3.24	1.32	1.38	1.33
16 × 16	324	1156	3.57	1.44	5.62	1.46
32 × 32	1156	4356	3.77	1.54	4.28	1.57
64 × 64	4356	16900	3.88	1.60	4.41	1.64
128 × 128	16900	66564	3.93	1.67	4.86	1.73

3. Approximation spaces in isogeometric analysis

In order to properly introduce the notation and to give a brief overview of how to construct the approximation spaces in isogeometric analysis, we recall the definition and some aspects of isogeometric analysis using B-splines, NURBS and LR B-splines basis functions and their geometry mappings in this section.

3.1. B-splines and NURBS

Given two positive integer p and n , we introduce the (ordered) knot vector

$$\Xi := \{\xi_1, \xi_2, \dots, \xi_{n+p+1}\} \text{ with } \xi_i \leq \xi_{i+1} \forall i, \quad (10)$$

where p is the degree of the B-spline and n is the number of basis functions (and control points) necessary to describe it. Here we allow repetition of knots, that is, $\xi_i \leq \xi_{i+1} \forall i$. The maximum multiplicity we allow is $p + 1$. In the following we will only work with open knot vectors, which means that first and last knots in Ξ have multiplicity $p + 1$. Given a knot vector Ξ , univariate B-spline basis functions $B_{i,p}(\xi)$, $i = 1, \dots, n$, are defined recursively by the well known Cox-de Boor recursion formula:

$$B_{i,0}(\xi) = \begin{cases} 1 & \text{if } \xi_i \leq \xi < \xi_{i+1}, \\ 0 & \text{otherwise.} \end{cases} \quad (11)$$

$$B_{i,p}(\xi) = \frac{\xi - \xi_i}{\xi_{i+p} - \xi_i} B_{i,p-1}(\xi) + \frac{\xi_{i+p+1} - \xi}{\xi_{i+p+1} - \xi_{i+1}} B_{i+1,p-1}(\xi) \quad \text{if } \xi_i \leq \xi < \xi_{i+1}, \quad (12)$$

where in (12), we adopt the convention $0/0 = 0$.

Let $B_{i,p}$ for $i = 1, \dots, n$ and $B_{j,q}$ for $j = 1, \dots, m$ are the B-spline basis functions of degree p and q defined by open knot vector $\Xi = \{\xi_1, \xi_2, \dots, \xi_{n+p+1}\}$ and $\Psi = \{\psi_1, \psi_2, \dots, \psi_{m+q+1}\}$, respectively. Then by means of tensor products, a multi-dimensional B-spline can be constructed as $B_{i,j}^{p,q}(\xi, \Psi) = B_{i,p}(\xi) \cdot B_{j,q}(\psi)$. In general, a rational B-spline in \mathbb{R}^d is the projection onto d -dimensional physical space of a polynomial B-spline defined in $(d - 1)$ -dimensional homogeneous co-ordinate space. Let $C_{ij} \in \mathbb{R}^2$ be the control points and $w_{ij} = (C_{ij}^w)_3$ are the positive weights given by projective control points $C_{ij}^w \in \mathbb{R}^3$. Then NURBS basis function on two dimensional parametric space $\hat{\Omega} = [0, 1]^2$ are defined as

$$R_{i,j}(\xi, \psi) = \frac{B_{i,p}(\xi) B_{j,q}(\psi) w_{ij}}{\sum_{\hat{i}=1}^n \sum_{\hat{j}=1}^m B_{\hat{i},p}(\xi) B_{\hat{j},q}(\psi) w_{\hat{i}\hat{j}}} \quad (13)$$

Observe that the continuity and support of NURBS basis function are the same as for B-splines. Furthermore, B-splines can be seen as a special case of NURBS with all weights being equal to one.

3.2. Local h -refinement using LR B-splines

In the following, we present briefly a class of Locally Refined (LR) B-splines space. For a more detailed presentation of the present class of LR B-splines we refer to the original contribution [27].

Local knot vectors

We have seen that a univariate spline basis function is constructed using a recursive formula of (11) and (12) with the global knot vector Ξ . However the support of a B-spline function, $B_{i,p}$, is contained in $[\xi_i, \xi_{i+p+1}]$ and these knots $\{\xi_i, \xi_{i+1}, \dots, \xi_{i+p+1}\}$ only contribute to the definition of $B_{i,p}$. Thus we do not need the global knot vector Ξ to define $B_{i,p}$, instead we can consider a *local knot vector*

$$\Xi_i = \{\xi_{i+j}\}_{j=0}^{p+1}, \quad \text{for } i = 1, \dots, n, \quad (14)$$

and use it in conjunction with (11) and (12) to define $B_{i,p}$, without altering the result. We have illustrated the basis functions given by local knots vectors Ξ_i s from $\Xi = [0, 0, 0, 1, 2, 3, 3, 4, 4, 4]$ in Figure 2.

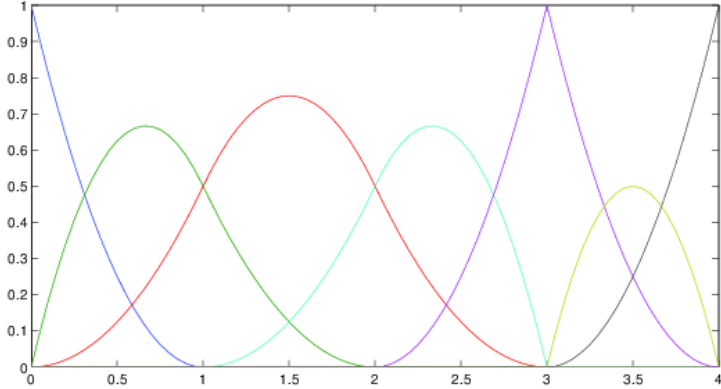


Figure 2: All quadratic basis functions generated by the knot $\Xi = [0, 0, 0, 1, 2, 3, 3, 4, 4, 4]$. Each individual basis function $B_{i,2}$ (represented by different colors) can be described using a local knot vector Ξ_i of length 4 described in (14).

Knot insertion

For local h -refinement, we again turn to existing spline theory. Tensor product B-splines form a subset of the LR B-splines and they obey the same core refinement ideas. From the tensor product B-spline theory we know that one might insert extra knots to enrich the basis without changing the geometric description. This comes from the fact that we have the available relation between B-splines in the old coarse spline space and in the new enriched spline space. For instance if we want to insert the knot $\hat{\xi}$ into the knot vector Ξ between the knots ξ_{i-1} and ξ_i , then the relation is defined by

$$B_\Xi(\xi) = \alpha_1 B_{\Xi_1}(\xi) + \alpha_2 B_{\Xi_2}(\xi), \quad (15)$$

where

$$\alpha_1 = \begin{cases} 1, & \xi_{p+1} \leq \hat{\xi} \leq \xi_{p+2} \\ \frac{\hat{\xi} - \xi_1}{\xi_{p+1} - \xi_1}, & \xi_1 \leq \hat{\xi} \leq \xi_{p+1} \end{cases} \quad (16)$$

$$\alpha_2 = \begin{cases} \frac{\xi_{p+2} - \hat{\xi}}{\xi_{p+2} - \xi_2}, & \xi_2 \leq \hat{\xi} \leq \xi_{p+2} \\ 1, & \xi_1 \leq \hat{\xi} \leq \xi_2 \end{cases} \quad (17)$$

and the knot vectors are $\Xi_1 = [\xi_1, \xi_2, \dots, \xi_{i-1}, \hat{\xi}, \xi_i, \dots, \xi_{p+1}]$ and $\Xi_2 = [\xi_2, \dots, \xi_{i-1}, \hat{\xi}, \xi_i, \dots, \xi_{p+1}, \xi_{p+2}]$.

To refine the bivariate B-spline basis function $B_{\Xi,\Psi}(\xi, \psi) = B_\Xi(\xi) \cdot B_\Psi(\psi)$ we consider the refinement of the basis function in one parametric direction at a time. By using the splitting algorithm of (15), when splitting in ξ -direction, we obtain

$$\begin{aligned} B_{\Xi,\Psi}(\xi, \psi) &= B_\Xi(\xi) \cdot B_\Psi(\psi) \\ &= (\alpha_1 B_{\Xi_1}(\xi) + \alpha_2 B_{\Xi_2}(\xi)) \cdot B_\Psi(\psi) \\ &= \alpha_1 B_{\Xi_1,\Psi}(\xi, \psi) + \alpha_2 B_{\Xi_2,\Psi}(\xi, \psi). \end{aligned}$$

Similarly, the splitting in another direction can be performed.

Now we define a weighted B-spline $B_{\Xi,\Psi}^\gamma(\xi, \psi) := \gamma B_{\Xi,\Psi}(\xi, \psi)$, where the weight factor $\gamma \in (0, 1]$. This is to ensure that LR B-splines maintain the partition of unity property, and it is noted that the weight factor γ is different from the rational weight w which is common in NURB representation. Refining a bivariate weighted B-splines becomes

$$B_{\Xi,\Psi}^\gamma(\xi, \psi) = \gamma B_{\Xi,\Psi}(\xi, \psi) \quad (18)$$

$$= \gamma \alpha_1 B_{\Xi_1,\Psi}(\xi, \psi) + \gamma \alpha_2 B_{\Xi_2,\Psi}(\xi, \psi) \quad (19)$$

$$= B_{\Xi_1,\Psi}^{\gamma_1}(\xi, \psi) + B_{\Xi_2,\Psi}^{\gamma_2}(\xi, \psi), \quad (20)$$

where $B_{\Xi_1, \Psi}^{\gamma_1}$ and $B_{\Xi_2, \Psi}^{\gamma_2}$ are new weighted B-spline basis functions with weights $\gamma_1 = \gamma\alpha_1$ and $\gamma_2 = \gamma\alpha_2$, respectively.

Local refinement algorithm

We now have the main ingredients to formulate the LR B-spline refinement rules. This will be implemented by keeping track of the mesh \mathcal{M}_ℓ at level ℓ and the spline space \mathcal{S}_ℓ . For each B-spline basis $B_{\Xi_k, \Psi_k}^{\gamma_k}$, where k is a single running global index, we store the following information:

- Ξ_k , Ψ_k -local knot vectors in each parametric directions
- γ_k -scaling weights and C_k -control points.

Throughout the refinement we aim at keeping the partition of unity and leaving the geometric mapping unchanged, i.e. $\sum_{\forall k} B_{\Xi_k, \Psi_k}^{\gamma}(\xi, \psi) = 1$ and $\mathbf{F}(\xi, \psi) = \sum_{\forall k} B_{\Xi_k, \Psi_k}^{\gamma}(\xi, \psi)C_k$ at all levels of refinements.

Assuming a meshline \mathcal{E} is inserted, the refinement process is characterized by two steps.

- **Step 1:** Split any B-spline which support is completely traversed by the *new* meshline - update the weights and control points
- **Step 2:** For all new B-splines, check if their support is completely traversed by any *existing* meshline.

On the basis of that the above characterization is fulfilled at each refinement level a local refinement algorithm (**Algorithm 1**) to construct the LR B-spline space is proposed in [27]. The "Update control points and weight" step is described when a parent basis function B_i split into two newly created B-spline functions B_1 and B_2 results of splitting by Eq.(18). If B_1 is not present in LR B-spline list then we add it to the list and set its weight and control points equal to its parent function, i.e. $\gamma_1^{new} = \alpha_1\gamma_i$ and $C_1^{new} = C_i$. While if the newly created function is already exists in our spline space then we just update its control points and weight such as $C_1^{new} := (C_1\gamma_1 + C_i\gamma_i\alpha_1)/(\gamma_1 + \gamma_i\alpha_1)$ and $\gamma_1^{new} := \gamma_1 + \gamma_i\alpha_1$. Finally we remove the old basis functions from the spline space.

Algorithm 1 Local refinement algorithm

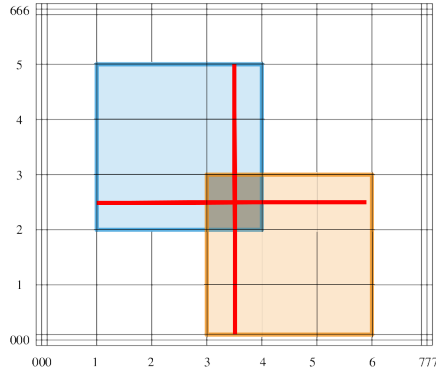
```

1: Input parameters: Spline space ( $\mathcal{S}$ ), LR mesh( $\mathcal{M}$ ), Meshline ( $\mathcal{E}$ )
2: for every B-spline  $B_i \in \mathcal{S}$  do
3:   if  $\mathcal{E}$  traverse support of  $B_i$  then
4:     refine  $B_i$  according to Eq. (18)
5:     Update control points  $C$  and weights  $\gamma$ 
6:   end if
7: end for
8: Update  $\mathcal{S}$  to  $\mathcal{S}_{new}$  and  $\mathcal{M}$  to  $\mathcal{M}_{new}$ 
9: for every existing  $B_i \in \mathcal{S}_{new}$  do
10:  for every edges  $\mathcal{E}_i \in \mathcal{M}_{new}$  do
11:    if  $\mathcal{E}_i$  traverse support of  $B_i$  then
12:      refine  $B_i$  according to Eq. (18)
13:      Update control points  $C$  and weights  $\gamma$ 
14:      (These steps may enlarge  $\mathcal{S}_{new}$  space further)
15:    end if
16:  end for
17: end for

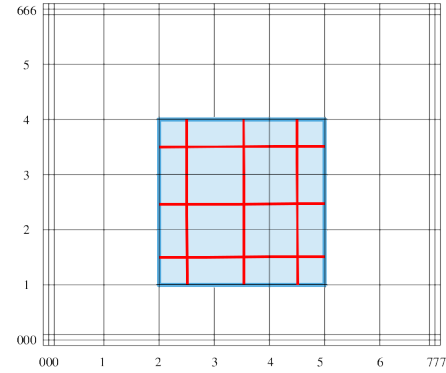
```

We now define an LR spline as an application of the local refinement algorithm **Algorithm 1**.

Definition 3.1 (LR spline). *An LR spline \mathcal{L} consist of $(\mathcal{M}, \mathcal{S})$, where \mathcal{M} is an LR mesh and \mathcal{S} is a set of LR B-splines defined on \mathcal{M} , and*



(a) Full span - split all functions on one element, here only two of all the nine functions with support on this element is depicted



(b) Structured Mesh - split all knot spans on one B-spline, notice that no bad aspect ratio elements are created

Figure 3: The ideas behind the different refinement strategies, here illustrated on a quadratic tensor product mesh. Notice the fundamental difference in that 3(a) is refining an element, while 3(b) is refining a B-spline.

- At each refinement level, $\mathcal{M}_{\ell+1} := \mathcal{M}_\ell \cup \mathcal{E}_\ell$, where \mathcal{E}_ℓ is a new meshline extension.
- $\mathcal{S}_\ell := \{B_{\Xi_k, \Psi_k}(\xi, \psi)\}_{k=1}^m$ is a set of all LR B-splines on \mathcal{M}_ℓ as a results of **Algorithm 1**.

In [27], the authors have illustrated two main isotropic h -refinement strategies as shown in Figure 3. A *full span* refinement strategy split an element with a knotline insertion which transverse through the support of every B-splines on the marked elements is shown in Figure 3(a). The idea of refining elements is a legacy from the finite element method where every inserted vertex would correspond to an additional degree of freedom. With LR B-splines this is not the case as the required length of the inserted meshlines may vary from element to element. Another way of refining LR B-splines is to identify the *B-spline* which should be refined instead of identifying which element. A strategy based on this approach denoted *structured mesh* refinement is shown in Figure 3(b) and the resulting mesh obtained through the use of structured mesh refinement strategy is said to be a *Structured LR Mesh* of degree (p, q) .

On the structured mesh of LR splines the following property holds:

Proposition 3.1. *A structured LR mesh of degree (p, q) is also a structured mesh of all degrees (\hat{p}, \hat{q}) , where $\hat{p} \leq p$ and $\hat{q} \leq q$.*

Proof. We here note that the definition of structured LR mesh is linked to the polynomial degree of the basis constructed on it. For tensor products, we have that every lower order function is completely contained in the support of a function of larger polynomial degree; in both directions. Due to Algorithm 1, when a larger B-spline split, we note that the lower order functions is split. Any B-spline of bi-degree (p, q) is thus guaranteed to contain enough functions of lower degree to span it's own support. \square

The above property will be useful in constructing the Serendipity pairing of discrete approximation spaces $S_h^{p,k}(\mathcal{M})$ - $S_h^{p+1,k+1}(\mathcal{M})$ using locally refined LR B-splines methodology of [27] in Section 4.

3.3. Geometry mappings

In particular, a single patch domain Ω is a NURBS region associated with the control points C_{ij} , and we introduce the geometrical map $\mathbf{F} : \hat{\Omega} \rightarrow \bar{\Omega}$ given by

$$\mathbf{F}(\xi, \psi) = \sum_{i=1}^n \sum_{j=1}^m C_{ij} R_{i,j}(\xi, \psi). \quad (21)$$

The above equation gives a B-spline region in a special case with all weights being equal to one. For our purpose we assume that the geometry mapping is continuous and bijective which are natural assumption for CAD applications.

Following the isoparametric approach, the space of B-splines and NURBS vector fields on the patch Ω is defined, component by component as the span of the push-forward of their respective basis function, e.g., in case of NURBS

$$V_h = \text{span}\{R_{i,j} \circ \mathbf{F}^{-1}, \text{ with } i = 1, \dots, n; j = 1, \dots, m\} \quad (22)$$

For LR B-splines, these will instead be defined over a single running global index k using the local knot vectors Ξ_k and Ψ_k (defined by a subsequences of global knot vectors Ξ and Ψ , respectively) by

$$\mathbf{F}(\xi, \psi) = \sum_{k=1}^{N_{dim}} \gamma_k C_k B_{\Xi_k, \Psi_k}(\xi, \psi), \quad (23)$$

where the local knot vectors based spline basis functions are defined by $B_{\Xi_k, \Psi_k}(\xi, \psi) = B_{\Xi_k}(\xi) \cdot B_{\Psi_k}(\psi)$ and γ_k is a weighting factor needed to obtain partition of unity, as discussed in Section 2.2. The isoparametric approach gives the space of LR B-splines vector fields on Ω by

$$V_h = \text{span}\{B_{\Xi_k, \Psi_k}(\xi, \psi) \circ \mathbf{F}^{-1}, \text{ with } k = 1, \dots, N_{dim}\}. \quad (24)$$

4. Serendipity pairing of discrete approximation spaces $S_h^{p,k}(\mathcal{M})$ - $S_h^{p+1,k+1}(\mathcal{M})$

In this section we explain and discuss the construction of Serendipity pairing of discrete isogeometric FE approximation spaces $S_h^{p,k}(\mathcal{M})$ - $S_h^{p+1,k+1}(\mathcal{M})$ using locally refined LR B-splines methodology of [27]. We first explain the basic differences in h -, p -, and k -refinements available in isogeometric analysis.

4.1. Basics about h -, p - and k -refinement

A univariate B-spline of degree $p = 1$ with knot vector $\Xi = \{0, 0, \frac{1}{3}, \frac{2}{3}, 1, 1\}$ is shown in Figure 4(a). It consists of three elements and four C^0 linear basis functions, i.e. the discrete FE space $S_h^{1,0}(\mathcal{M})$, which may be refined (or enriched) by three different approaches: h -, p - and k -refinement shown in Figure 4(b), (c), and (d), respectively. The corresponding discrete isogeometric FE spaces are $S_{h/2}^{p,k}(\bar{\mathcal{M}})$, $S_h^{p+1,k}(\mathcal{M})$, and $S_h^{p+1,k+1}(\mathcal{M})$, respectively. Thus, by doing h -refinement we obtain seven C^0 linear basis functions with halved element size (therefore $h/2$ and $\bar{\mathcal{M}}$ in $S_{h/2}^{p,k}(\bar{\mathcal{M}})$), whereas we for p -refinement obtain six C^0 quadratic splines without changing the mesh. Both the h - and p -refinement shown here is identical to what is done using classical C^0 Lagrange finite elements, but in isogeometric analysis we have one more option to play with and that is the interelement regularity. Thus, we might combine order elevation with increasing the regularity accordingly, i.e. increase $p \rightarrow p+1$ and $k \rightarrow k+1$ simultaneously, and this is denoted k -refinement. In Figure 4(d) we see that by doing k -refinement we obtain five C^1 quadratic splines.

To illustrate k -refinement for 2D we show in first row of Figure 5 a set of bi-variate tensorial meshes. Let $\Xi^1 = \Xi^2 = \{0, 0, 0, 1/8, 1/4, 3/8, 1/2, 5/8, 3/4, 7/8, 1, 1, 1\}$ be two given knot vectors and $S_h^{p,k}$ with $h = 1/8, p = 2, k = 1$ be the quadratic spline space generated by these knot vectors as shown in Figure 5(a). The tensorial meshes displayed in the right is the mesh obtained by k -refinement of the mesh to the left. Thus, the first row of Figure 5 shows Serendipity pairings of isogeometric FE approximation spaces $S_h^{2,1}$ - $S_h^{3,2}$ on given mesh \mathcal{M}_0 . The basis functions generated on these meshes are illustrated by means of the location of the Greville abscissa points defined by an average of internal local knot vectors with respect to each basis functions. A more detailed information about these types of refinements available in isogeometric analysis can be obtained from [15].

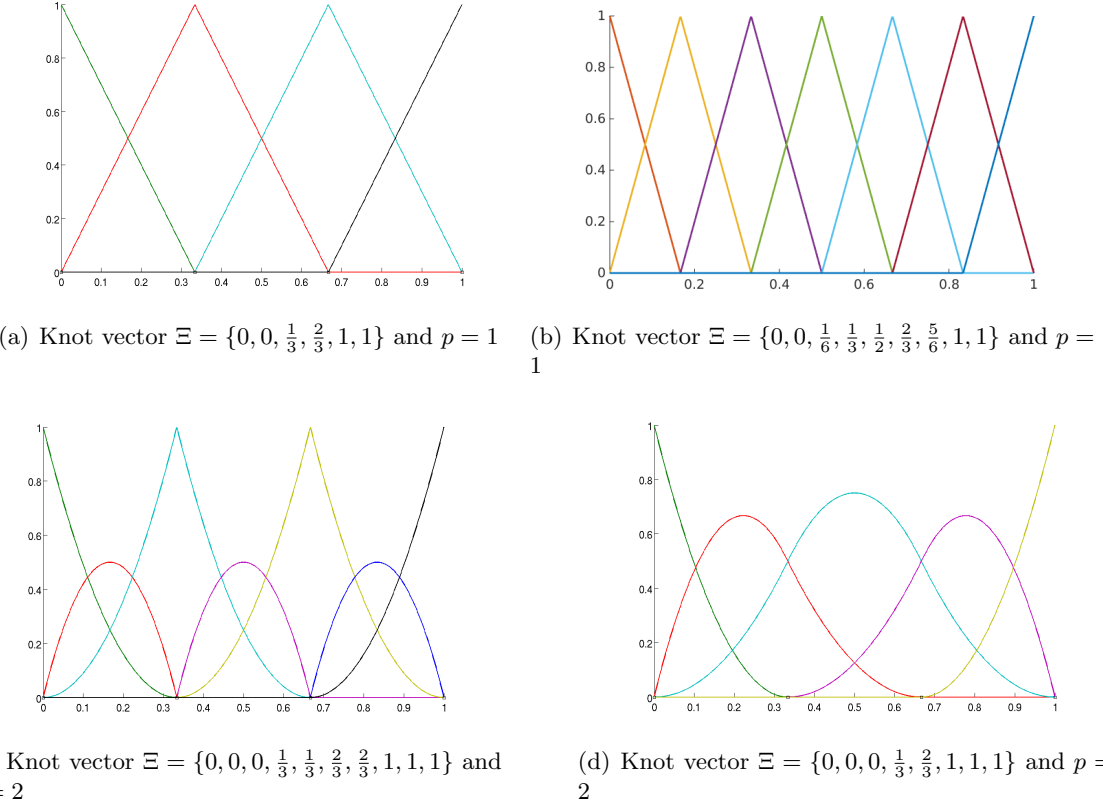


Figure 4: **Different types of refinements in IGA** : (a) Linear splines obtain from knot vector $\Xi = \{0, 0, \frac{1}{3}, \frac{2}{3}, 1, 1\}$ (corresponding space denoted $S_h^{1,0}(\mathcal{M})$), (b) h-refinement ($S_{h/2}^{1,0}(\bar{\mathcal{M}})$) , (c) p-refinement ($S_h^{p+1,k}(\mathcal{M})$), (d) k-refinement ($S_h^{p+1,k+1}(\mathcal{M})$).

4.2. Algorithm for Serendipity pairing using k -refinement in an adaptive setting

To construct the Serendipity paring of isogeometric FE approximation spaces $S_h^{p,k}(\mathcal{M})$ - $S_h^{p+1,k+1}(\mathcal{M})$ in an adaptive setting, we consider the *structured mesh* refinement strategy of LR B-splines [27] as shown in Figure 3(b). In our adaptive isogeometric analysis, we start the refinement procedure from a tensorial mesh and then the mesh is adapted using the structured mesh refinement strategy of [27]. To decide which basis functions to refine we make use of a posteriori error estimators that is typically computed on each element. We transfer this information from elements to basis functions by adding the element errors for all elements in the support of each basis function.

The complete procedure to construct the Serendipity paring of isogeometric FE approximation spaces $S_h^{p,k}(\mathcal{M})$ - $S_h^{p+1,k+1}(\mathcal{M})$ in adaptive isogeometric setting is given by the following algorithm:

Algorithm 2 Discrete pair of $S_h^{p,k}(\mathcal{M})$ - $S_h^{p+1,k+1}(\mathcal{M})$ spaces

Input parameters: Spline spaces $S_h^{p,k}(\mathcal{M}_0)$, $S_h^{p+1,k+1}(\mathcal{M}_0)$, initial tensorial LR mesh(\mathcal{M}_0)

for each level (ℓ) of refinement steps

Select some percentage of B-spline functions $B_i \in S_h^{p+1,k+1}(\mathcal{M}_\ell)$ using given error indicator

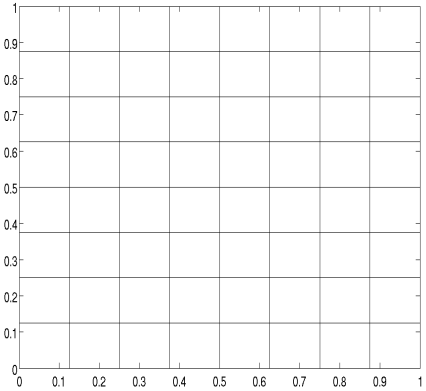
Refine selected B-spline functions of using Algorithm 1 to obtain $S_h^{p+1,k+1}(\mathcal{M}_{\ell+1})$

Store the information about Meshline of length $p + 2$ in \mathcal{E}_ℓ

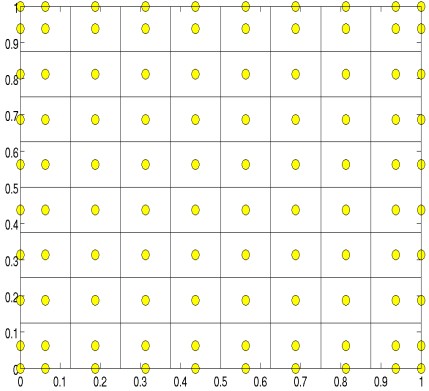
Refine every B-spline $B_i \in S_h^{p,k}(\mathcal{M}_\ell)$ using the the Meshline \mathcal{E}_ℓ and **Algorithm 1**.

end for

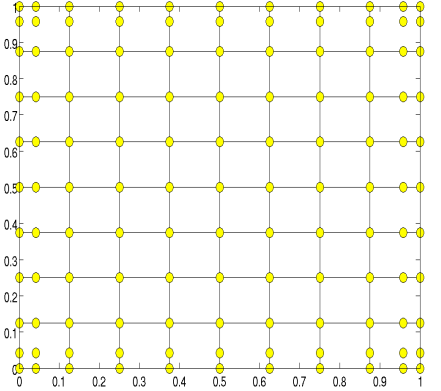
To illustrate Algorithm 2 we have in Figure 5 displayed the obtained Serendipity pairings of isogeometric FE approximation spaces $S_h^{2,1}(\mathcal{M}_\ell)$ - $S_h^{3,2}(\mathcal{M}_\ell)$ in adaptive setting by means of local h -refinements using LR B-splines. The algorithm starts with the tensorial mesh displayed in Figure 5(a) with the corresponding Serendipity paring of quadratic and cubic LR B-splines spaces as shown in first row of Figure 5(b)-(c). Notice that the integration



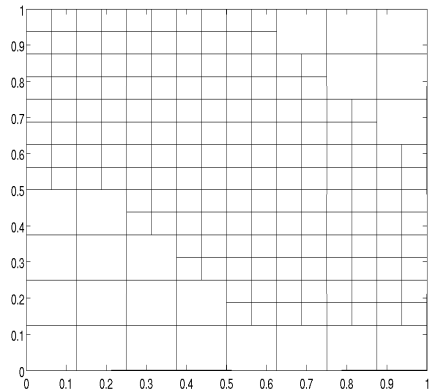
(a) Initial mesh \mathcal{M}_0



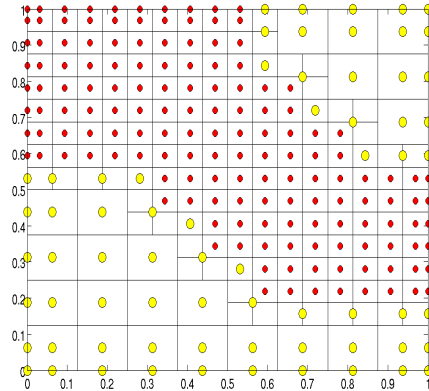
(b) $\mathcal{S}_h^{2,1}(\mathcal{M}_0)$, Degrees of freedom 100



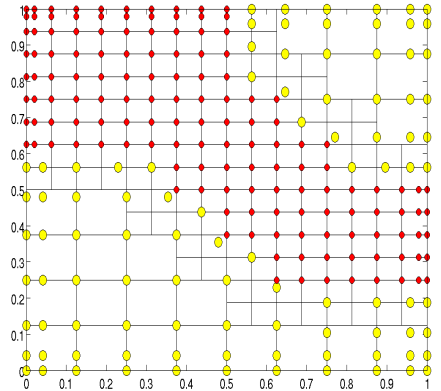
(c) $\mathcal{S}_h^{3,2}(\mathcal{M}_0)$, Degrees of freedom 121



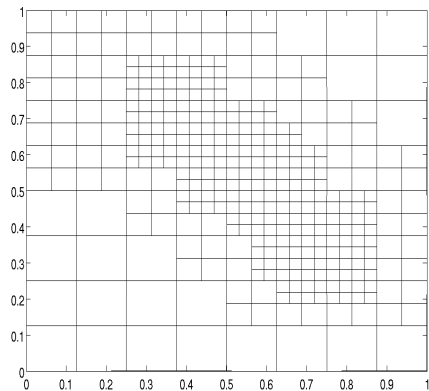
(d) After one refinement step, \mathcal{M}_1



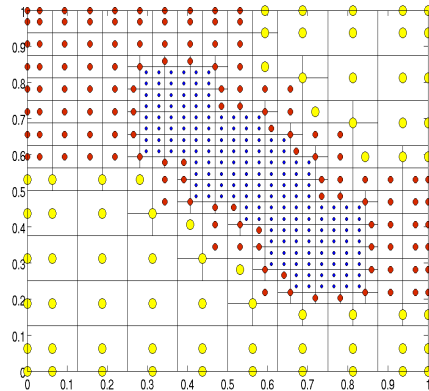
(e) $\mathcal{S}_h^{2,1}(\mathcal{M}_1)$, Degrees of freedom 219



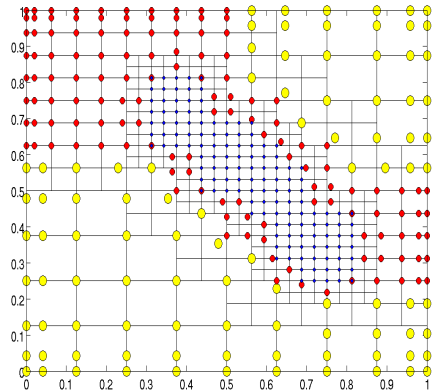
(f) $\mathcal{S}_h^{3,2}(\mathcal{M}_1)$, Degrees of freedom 238



(g) After two refinement steps, \mathcal{M}_2



(h) $\mathcal{S}_h^{2,1}(\mathcal{M}_2)$, Degrees of freedom 366



(i) $\mathcal{S}_h^{3,2}(\mathcal{M}_2)$, Degrees of freedom 364

Figure 5: Serendipity pairing of approximation spaces with LR B-splines: Left column represents the LR adaptive mesh obtained from three step of local h -refinement, Middle column represent the case of quadratic LR isogeometric elements $\mathcal{S}_h^{2,1}$, and right column represents the cubic LR isogeometric elements $\mathcal{S}_h^{3,2}$ which can be seen as k-refined version of quadratic LR spline elements of middle column.

Table 3: Dimensions for $\mathcal{S}_h^{2,1}(\mathcal{M})$ from Figure 5 and their h -, p -, and k -refined spaces.

Adaptive steps	h-refinement			p-refinement		k-refinement	
	$\dim \mathcal{S}_h^{2,1}$	$\dim \mathcal{S}_{h/2}^{2,1}$	$r_h = \frac{\dim \mathcal{S}_{h/2}^{2,1}}{\dim \mathcal{S}_h^{2,1}}$	$\dim \mathcal{S}_h^{3,1}$	$r_p = \frac{\dim \mathcal{S}_h^{3,1}}{\dim \mathcal{S}_h^{2,1}}$	$\dim \mathcal{S}_h^{3,2}$	$r_k = \frac{\dim \mathcal{S}_h^{3,2}}{\dim \mathcal{S}_h^{2,1}}$
0	100	324	3.24	324	3.24	121	1.21
1	219	1132	5.16	1132	5.16	238	1.08
2	366	1860	5.08	1860	5.08	364	0.99

 Table 4: Dimensions for $\mathcal{S}_h^{3,2}(\mathcal{M})$ on meshes similar to Figure 5 and their h -, p -, and k -refined spaces.

Adaptive steps	h-refinement			p-refinement		k-refinement	
	$\dim \mathcal{S}_h^{3,2}$	$\dim \mathcal{S}_{h/2}^{3,2}$	$r_h = \frac{\dim \mathcal{S}_{h/2}^{3,2}}{\dim \mathcal{S}_h^{3,2}}$	$\dim \mathcal{S}_h^{4,2}$	$r_p = \frac{\dim \mathcal{S}_h^{4,2}}{\dim \mathcal{S}_h^{3,2}}$	$\dim \mathcal{S}_h^{4,3}$	$r_k = \frac{\dim \mathcal{S}_h^{4,3}}{\dim \mathcal{S}_h^{3,2}}$
0	121	361	2.98	361	2.98	144	1.19
1	292	1483	5.09	1483	5.09	320	1.10
2	502	2377	4.73	2377	4.77	513	1.02

LR mesh for the pair of isogeometric spaces $S_h^{2,1}(\mathcal{M}_\ell)$ - $S_h^{3,2}(\mathcal{M}_\ell)$ will be the same. Here we choose to first transfer the element error information obtained by the given indicator to the basis functions of the space $S_h^{3,2}(\mathcal{M}_\ell)$. Then some percentage of the basis functions of this space are refined using the structured mesh refinement strategy in Algorithm 1. The information about the new inserted Meshline of length $(p+2)$ at each steps ℓ s are stored in \mathcal{E}_ℓ . Based on these information we then refine the basis functions of $S_h^{2,1}(\mathcal{M}_\ell)$. By performing the refinement this way a Serendipity pairing of spaces $S_h^{2,1}(\mathcal{M}_\ell)$ - $S_h^{3,2}(\mathcal{M}_\ell)$ is obtained at each refinement levels. The Meshline of length $(p+2)$ will make sure that the h -refinement is proper both in the space $S_h^{2,1}(\mathcal{M}_\ell)$ along with its k -refined counterparts.

In adaptive isogeometric analysis using LR B-spline we noticed that the dimension of spline space $S_h^{p+1,k+1}(\mathcal{M}_\ell)$ could be less (equal, or more) than the dimension of spline space $S_h^{p,k}(\mathcal{M}_\ell)$, while on tensorial meshes we know for fact that the dimension of $S_h^{p+1,k+1}(\mathcal{M}_\ell)$ will be always larger than $S_h^{p,k}(\mathcal{M}_\ell)$. However, in both cases the dimension are almost equal and the difference is very small in comparison to their h - and p -refined discrete pair counterpart. This is illustrated in Tables 3-5 for quadratic C^1 LR B-splines, cubic C^2 LR B-splines, and quartic C^3 LR B-splines on three adapted LR meshes of Figure 5, respectively.

Remark 4.1. In case of h -refinement and p -refinement the Serendipity pairing of isogeometric approximation spaces $S_h^{p,k}(\mathcal{M})$ - $S_{h/2}^{p,k}(\bar{\mathcal{M}})$ and $S_h^{p,k}(\mathcal{M})$ - $S_h^{p+1,k}(\mathcal{M})$, respectively, satisfy

$$S_h^{p,k}(\mathcal{M}) \subset S_{h/2}^{p,k}(\bar{\mathcal{M}}) \quad \text{and} \quad S_h^{p,k}(\mathcal{M}) \subset S_h^{p+1,k}(\mathcal{M}), \quad (25)$$

while for the k -refined discrete spaces $S_h^{p,k}(\mathcal{M})$ - $S_h^{p+1,k+1}(\mathcal{M})$ we have

$$S_h^{p,k}(\mathcal{M}) \not\subset S_h^{p+1,k+1}(\mathcal{M}) \quad \text{and} \quad S_h^{p,k}(\mathcal{M}) \not\supset S_h^{p+1,k+1}(\mathcal{M}). \quad (26)$$

Remark 4.2. The integration LR mesh at each refinement level will be same for both the spaces $S_h^{p,k}(\mathcal{M}_\ell)$ and $S_h^{p+1,k+1}(\mathcal{M}_\ell)$ and at each refinement level they satisfy the following nestedness behavior

$$S_h^{p,k}(\mathcal{M}_\ell) \subset S_h^{p,k}(\mathcal{M}_{\ell+1}) \quad \text{and} \quad S_h^{p+1,k+1}(\mathcal{M}_\ell) \subset S_h^{p+1,k+1}(\mathcal{M}_{\ell+1})$$

5. Error estimation

5.1. Model problem

The model problem is Poisson's equation on a open bounded two dimensional domain $\Omega \in \mathbb{R}^2$ with Lipschitz boundary $\Gamma = \Gamma_D \cup \Gamma_N$, where Γ_D and Γ_N are the Dirichlet and Neumann boundaries, respectively. The *strong* form of the boundary value problem: Find the displacement $u : \bar{\Omega} \rightarrow \mathbb{R}$ such that

Table 5: Dimensions for $\mathcal{S}_h^{4,3}(\mathcal{M})$ on meshes similar to Figure 5 and their h -, p -, and k -refined spaces.

Adaptive steps	$\dim \mathcal{S}_h^{4,3}$	h-refinement		p-refinement		k-refinement	
		$\dim \mathcal{S}_{h/2}^{4,3}$	$r_h = \frac{\dim \mathcal{S}_{h/2}^{4,3}}{\dim \mathcal{S}_h^{4,3}}$	$\dim \mathcal{S}_h^{5,3}$	$r_p = \frac{\dim \mathcal{S}_h^{5,3}}{\dim \mathcal{S}_h^{4,3}}$	$\dim \mathcal{S}_h^{5,4}$	$r_k = \frac{\dim \mathcal{S}_h^{5,4}}{\dim \mathcal{S}_h^{4,3}}$
0	144	400	2.77	400	2.77	169	1.17
1	484	2260	4.67	2260	4.67	498	1.03
2	699	3476	4.80	3476	4.80	724	1.04

$$-\Delta u = f \text{ on } \Omega; \quad (27)$$

$$u = 0 \text{ on } \Gamma_D; \quad (28)$$

$$\mathbf{n} \cdot \nabla u = g \text{ on } \Gamma_N. \quad (29)$$

The data are assumed to be sufficiently smooth, that is, $f \in L^2(\Omega)$, $g \in L^2(\Gamma_N)$ and \mathbf{n} is the unit outward normal vector to Γ . An equivalent formulation of the boundary value problem is the variational formulation seeking $u \in V$ such that

$$a(u, v) = \ell(v) \quad \forall v \in V, \quad (30)$$

where the trial and test space V is the usual Sobolev space of functions from $H^1(\Omega)$ whose trace vanishes on the Dirichlet part of the boundary and is defined by $V := \{v \in H^1(\Omega) : v = 0 \text{ on } \Gamma_D\}$.

The form $a(u, v)$ is assumed to be a V -coercive bilinear form on $V \times V$ and the linear functional $\ell(v)$ is an element of the dual space V' , given as

$$a(u, v) = \int_{\Omega} \nabla u \cdot \nabla v d\Omega \quad \text{and} \quad \ell(v) = \int_{\Omega} f v d\Omega + \int_{\Gamma_N} g v ds. \quad (31)$$

The existence and uniqueness of the solution to this continuous problem is guaranteed by the Lax-Milgram theorem. The Galerkin finite element approximation to this variational problem may then be given as follow: Given a finite-dimensional subspace $V_h \subset V$ and $\ell \in V'$, find $u_h \in V_h$ such that

$$a(u_h, v_h) = \ell(v_h) \quad \forall v_h \in V_h. \quad (32)$$

In isogeometric setting, the discrete space V_h formed with B-splines/NURBS and LR B-splines are given by (22) and (24), respectively.

Let u be the exact solution and u_h be the isogeometric FE solution. The discretization errors are denoted by

$$e(\mathbf{x}) = u(\mathbf{x}) - u_h(\mathbf{x}), \quad e_{\sigma}(\mathbf{x}) = \nabla u(\mathbf{x}) - \nabla u_h(\mathbf{x}), \quad (33)$$

where e is the error in the displacement u_h and e_{σ} is the error in the gradient ∇u_h . We now introduce the following error norms:

$$\|e\|_{L^2(\Omega)} := \|u - u_h\|_{L^2(\Omega)} = \left(\int_{\Omega} (u - u_h)^2 d\Omega \right)^{1/2} \quad (34)$$

$$\|e\|_E : \sqrt{a(e, e)} = |e|_{H_0^1(\Omega)} = \|e_{\sigma}\|_{L^2(\Omega)} = \left(\int_{\Omega} (\nabla u - \nabla u_h)^T \cdot (\nabla u - \nabla u_h) d\Omega \right)^{1/2} \quad (35)$$

5.2. A priori error estimation

In classical FEA, the fundamental error estimate for the elliptic boundary value problem, expressed as a bound on the difference between the exact solution, u , and the FEA solution, u_h , takes the form

$$\|u - u_h\|_m \leq C_{\text{FEA}} h^{\beta} \|u\|_r \quad (36)$$

where $\|\cdot\|_k$ is the norm corresponding to the Sobolev space $H^k(\Omega)$, h is a characteristic length scale related to the size of the element in the mesh and $\beta = \min(p+1-m, r-m)$ where p is the polynomial degree of the basis, and C_{FEA} is a constant that does not depend on u and h . The parameter r describe the regularity of the exact solution u and $2m$ is the order of the differential operator of the corresponding PDE.

The basic a priori error estimate results analogous to (36) for NURBS based isogeometric method (cf. [7]) is given as follows: for $u \in H^r(\Omega)$ with $0 \leq m \leq r \leq p+1$ and $u_h \in V_h$:

$$\|u - u_h\|_m \leq C_{\text{IGA}} h^\beta \|u\|_r, \quad \text{where } \beta = \min(p+1-m, r-m). \quad (37)$$

For the uniform h -refinement, one sees from (36) and (37) that the isogeometric solution obtained using C^{p-1} NURBS of degree p converges at same rate as FEA polynomial of degree p . However, provided that $C_{\text{IGA}} < C_{\text{FEA}}$, IGA may be more efficient (i.e. accurate) in terms of degrees of freedom (N_{dof}), and this is often the case in practice.

5.3. A posteriori error estimation

The standard a priori error estimate for the exact error given in previous section tells us about the rate of convergence which we can anticipate but is of limited use if we wish to find a numerical estimate of the accuracy. One way in which we might get a realistic estimate or bound upon the discretization error is to use the approximation solution u_h itself in estimating $\|e\|_E$. The idea of using u_h to estimate the error is called *a posteriori error estimation* and some variety of methods to use it have been seen in literature, see [2] and [39] for detailed survey on this topic.

Now we design a simple posteriori error estimators in adaptive isogeometric analysis, the employed technique is based on solving the original problem with two discretization schemes of different accuracy and using the difference in the approximations as an estimate of the error. Consider the elliptic model problems of (27)-(29) and suppose the numerical approximation u_h in FE subspace V_h is known. Let u_h^* be an approximation of elliptic problem (27)-(29) from the k -refined FE subspace V_h^* , then the energy error can be written as

$$\|e\|_E = \|u - u_h\|_E \leq \underbrace{\|u_h^* - u_h\|_E}_{\text{Computable}} + \underbrace{\|u - u_h^*\|_E}_{\text{Non-computable}}. \quad (38)$$

Let us consider the right hand side part of (38) as the exact error estimate defined by

$$\eta_h^{EX} = \|u_h^* - u_h\|_E + \|u - u_h^*\|_E, \quad (39)$$

which will show us the role of the triangle inequality in estimating the exact error using (38).

Next, If u_h^* is superior to the original approximation u_h then the difference between the two approximations $\|u_h^* - u_h\|_E$ will provide a computable estimate for the exact error

$$\|e\|_E \approx \|u_h^* - u_h\|_E = \eta_h^*. \quad (40)$$

In Eq.(40), the second term from (39) is neglected completely on the basis that it should be small in comparison to the first term and η_h^* is used as an estimate of the error. However, the term η_h^* does not provide a *guaranteed* upper bound in general as shown by our numerical results in Section 6. Here we consider a simple explicit residual based error estimate to get an upper bound on the term $\|u - u_h^*\|_E$, see [26, 38], and a complete error estimate from (38) then becomes

$$\eta_h^{RES} = \|u_h^* - u_h\|_E + C_{\text{RES}} \left\{ \sum_{\forall K \in \mathcal{M}} h_K^2 \|R\|_{L^2(K)}^2 + \frac{1}{2} h_K \|J\|_{L^2(\partial K)}^2 \right\}^{1/2}, \quad (41)$$

where h_K is the diameter of element $K \in \mathcal{M}$, $R = f + \Delta u_h^*$ defined the interior residual and J defined the boundary residual $J|_\gamma = g - \frac{\partial u_h^*}{\partial n}$ for $\gamma \in \partial K \cap \partial \Gamma_N$ and the jump term $J|_\gamma = -\frac{1}{2} \left[\frac{\partial u_h^*}{\partial n} \right]$ for $\gamma \in \partial K$. The contribution of element jump discontinuity term becomes zeros for smooth spline approximation spaces, which generally have at least C^1 -continuity across the element boundaries. The error constant C_{RES} in (41) comes from the Clement-type

interpolation operators. Such constant are mesh (element) dependent and often incomputable for general element shape. A global constant can overestimate the local constants, and thus the exact error. We assume the value of constant $C_{\text{RES}} = 1$ in the computation of numerical results of Section 6.

Saturation assumption

The effectiveness of the approximation $\|e\|_E \approx \|u_h^* - u_h\|_E$ is dictated by whether u_h^* really does represent an improved approximation over the approximation u_h . This notion is quantified in terms of the saturation assumptions, i.e. there exist a constant $C_{\text{sat}} \in [0, 1)$ such that

$$\|u - u_h^*\|_E \leq C_{\text{sat}} \|u - u_h\|_E. \quad (42)$$

It is easy to see that the saturation condition (42) will hold for *reasonable* functions u . For example, suppose that the Galerkin subspace $V_h = S_h^{2,1}(\mathcal{M})$ consists of quadratic C^1 splines basis functions and its k -refined subspace $V_h^* = S_h^{3,2}(\mathcal{M})$ consists of cubic C^2 splines basis functions.

(i) If the solution u is smooth, say $u \in H^4(\Omega)$, then a priori error estimates from (37) imply that on quasi-uniform meshes of size h , we have

$$\|u - u_h\| \leq C_1 h^2 \|u\|_{H^3(\Omega)} \quad \text{and} \quad \|u - u_h^*\| \leq C_2 h^3 \|u\|_{H^4(\Omega)}. \quad (43)$$

Therefore, asymptotically, we obtain that $C_{\text{sat}} = O(h)$ —a much stronger behaviour than that is required for the saturation assumption.

(ii) If the solution u is not sufficiently smooth, say $u \in H^\lambda(\Omega)$, $\lambda \in [1, 2)$, examples are problems with singularities within the solution domain or on its boundary, then a priori error estimates from (37) imply that on quasi-uniform meshes of size h , we have

$$\|u - u_h\| \leq C_3 h^{\alpha_1} \|u\|_{H^{\alpha_1+1}(\Omega)} \quad \text{and} \quad \|u - u_h^*\| \leq C_4 h^{\alpha_2} \|u\|_{H^{\alpha_2+1}(\Omega)}, \quad (44)$$

where the value of the non-negative real parameter α_i s depends on how the family of meshes \mathcal{M} are created. Assume that λ is a real number characterizing the strength of the singularity. For a sequence of uniformly, or nearly uniformly, refined meshes we then have

$$\alpha_1 = \min\{2, \lambda\} \quad \text{and} \quad \alpha_2 = \min\{3, \lambda\}. \quad (45)$$

Thus, when $\lambda < p$ the rate of convergence is limited by the strength of the singularity, and not on the polynomial degree p . In isogeometric analysis, the constant C_{IGA} present in a priori error estimates (37) depends on degree p and the shape (but not size) of the domain Ω , as well as the shape regularity of the mesh, see [7]. A clear argument about its dependence on p for C^{p-1} smooth isogeometric element case is not known while some partial results for reduce continuity order isogeometric elements are presented in [9]. Thus the constants C_3 and C_4 present in (44) also depend on the degree of approximations. Numerically we observed that both approximation u_h and u_h^* will provide the same rate of convergence but the results for u_h^* will be more accurate than u_h . Hence on some coarse meshes for the problem with singularity we observed $C_{\text{sat}} < 1$, and asymptotically with adaptive h -refinement steps, we are able to create the family of meshes where we obtain that $C_{\text{sat}} = O(h)$.

Remark 5.1. *We numerically illustrate in Section 6 that the above two arguments about the saturation assumption (42) will holds true for the case of elliptic problems with smooth and non-smooth solution.*

Remark 5.2. *Despite the above arguments on the saturation assumption, we want to point out that the saturation assumption will fail to be true in general. For example, let the exact solution $u \in S_h^{2,1}(\mathcal{M})$ on a given mesh \mathcal{M} with C^1 -continuity across element boundaries and we consider $V_h = S_h^{2,1}(\mathcal{M})$ and $V_h^* = S_h^{3,2}(\mathcal{M})$ in the error estimate (40). Then the error in $u_h \in S_h^{2,1}(\mathcal{M})$ approximation will be zero, i.e. $\|u - u_h\|_E = 0$, while there will be some errors in $u_h^* \in S_h^{3,2}(\mathcal{M})$ and the saturation assumption will fail in this particular case. Such problem can also arise by taking some classes of data of problem f such that the approximations u_h and u_h^* belong to the finite-dimensional FE spaces*

and so the component of data f that is orthogonal (in an L_2 sense) to the spaces is essentially invisible, see Chapter 5 of [2]. Fortunately, the data in practical computations are taken from quite restricted sets such as global polynomials or piecewise analytical functions, so that the saturation assumption may be quite realistic in a practical setting.

6. Numerical results

In this section, we first introduce the nomenclature used and the aim of our numerical studies. Then we consider two elliptic benchmark problems with analytical known solution u to demonstrate the effectiveness of the proposed error estimators. Finally we report some preliminary results obtained with an even more cost effective approach.

6.1. Nomenclature

Error measures

The effectiveness of the various error estimators is assessed by evaluating how well they are able to estimate the relative errors (%) in energy norm

$$\|e\|_{RE} = \frac{\|u - u_h\|_E}{\|u\|_E} \times 100\%, \quad \text{for } u_h \in \mathcal{S}_h^{p,k}(\mathcal{M}), \quad (46)$$

$$\|e^*\|_{RE} = \frac{\|u - u_h^*\|_E}{\|u\|_E} \times 100\%, \quad \text{for } u_h^* \in \mathcal{S}_h^{p+1,k+1}(\mathcal{M}). \quad (47)$$

Furthermore, let $\|e\|_E$ and $\|e\|_{E(\Omega_{el})}$ be the global and element error, respectively. Then we define the root mean square of the exact element errors by:

$$\|e\|_{RMS} = \frac{\left(\frac{1}{N_{el}} \sum_{el=1}^{N_{el}} (\|e\|_{E(\Omega_{el})} - \|e\|_{avg})^2 \right)^{1/2}}{\|e\|_{avg}}, \quad (48)$$

where the average exact element error is defined as

$$\|e\|_{avg} = \frac{1}{N_{el}} \sum_{el=1}^{N_{el}} \|e\|_{E(\Omega_{el})}. \quad (49)$$

The root mean square of the exact element errors given in Equation (48) measures the deviation from an uniform element error distribution. A mesh giving uniform element error distribution is considered to be optimal for which we have that $\|e\|_{RMS} = 0$. Thus, we refer to asymptotically optimal mesh refinement procedure when a sequence of meshes satisfying $\lim_{h \rightarrow 0} \|e\|_{RMS} = 0$.

Error estimators

In the present adaptive methodology we consider the following error estimators $\eta_h^{(\cdot)}, \cdot = \{\text{EX}, *, \text{RES}\}$ of Section 5:

$$\eta_h^{\text{EX}} = \|u_h^* - u_h\|_E + \|u - u_h^*\|_E, \quad (50)$$

$$\eta_h^* = \|u_h^* - u_h\|_E, \quad (51)$$

$$\eta_h^{\text{RES}} = \|u_h^* - u_h\|_E + \left\{ \sum_{\forall K \in \mathcal{M}} h_K^2 \|R\|_{L^2(K)}^2 + \frac{1}{2} h_K \|J\|_{L^2(\partial K)}^2 \right\}^{1/2}. \quad (52)$$

Effectivity index (θ)

The effectivity indices that measures the quality of error estimators are defined by

$$\theta^{(\cdot)} = \frac{\eta_h^{(\cdot)}}{\|e\|_E} \quad \text{for } (\cdot) = \{\text{EX}, *, \text{RES}\}. \quad (53)$$

and we refer to $\eta_h^{(\cdot)}$ as an asymptotically exact error estimators if $\lim_{h \rightarrow 0} \theta^{(\cdot)} = 0$.

Saturation constant (C_{sat})

For the higher order approximation u_h^* we compute the saturation constant C_{sat} , defined by

$$C_{\text{sat}} = \frac{\|u - u_h^*\|_E}{\|u - u_h\|_E}. \quad (54)$$

In order to get reliable error estimates the saturation constant should satisfy $C_{\text{sat}} \in [0, 1]$. Furthermore, to obtain asymptotically exact error estimator the saturation constant have to fulfill $C_{\text{sat}} = O(h^\alpha)$ for some $\alpha > 0$.

Marking strategy

The marking strategy, that is, the method of how to choose the basis functions for refinement in structured mesh refinement is the *Fixed iteration* strategy. Thus, in the adaptive refinement procedure, we always choose to refine a fixed percentages of those basis functions which contributes with most error in the isogeometric FE computation. It is recommend to use some small percentages say $\gamma < 5\%$ to achieved a proper adaptive refinement process resulting in optimal convergence rates. For the numerical results in this article we have been using $\gamma = 3\%$.

6.2. Aim of the numerical studies

The aim of numerical studies is to investigate whether for smooth problems with uniform mesh refinement we obtain:

- A higher convergence rate for u^* compared to u^h
- asymptotically exact error estimate for η_h^* on refined meshes
- conservative error estimate with η_h^{RES}

and for non-smooth problems with adaptive mesh refinement we obtain:

- Optimal convergence rate, i.e. $O(h^p)$ for u^h measured in energy norm
- a higher convergence rate for u^* compared to u^h
- asymptotically exact error estimate for η_h^* on adaptive refined meshes
- conservative error estimate with η_h^{RES}
- asymptotically optimal element error distribution

6.3. Uniform refinement results

Example 1. (Sinus problem) Consider the following two dimensional elliptic problem

$$-\Delta u = f \quad \text{in } \Omega, \quad (55)$$

with homogenous boundary conditions

$$u = 0 \quad \text{on } \partial\Omega. \quad (56)$$

Here $\Omega = (0, 1)^2$ is a square domain and f is constructed to correspond to the exact solution

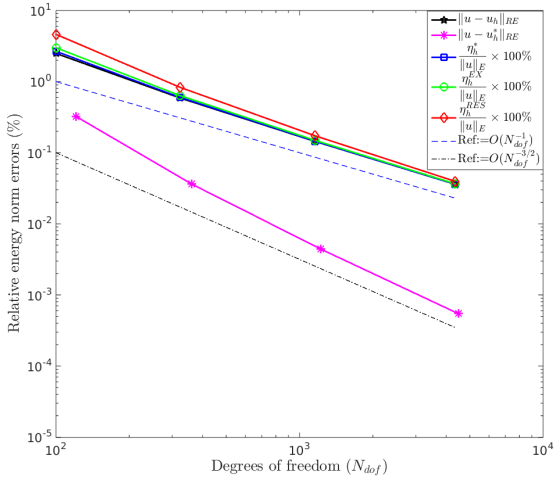
$$u(x, y) = \sin(2\pi x) \sin(2\pi y). \quad (57)$$

The error plots for the comparison of relative error (%) in energy norm and effectivity indeces $\theta^{(\cdot)}, \cdot = \{\ast, RES, EX\}$ using the approximation spaces $V_h := \mathcal{S}_h^{p,p-1}$ and k -refined spaces $V_h^* := \mathcal{S}_h^{p+1,p}$ for $p = 2, 3, 4$ (respectively in each row) with uniform h -refinements for Example 1 are shown in Figure 6.

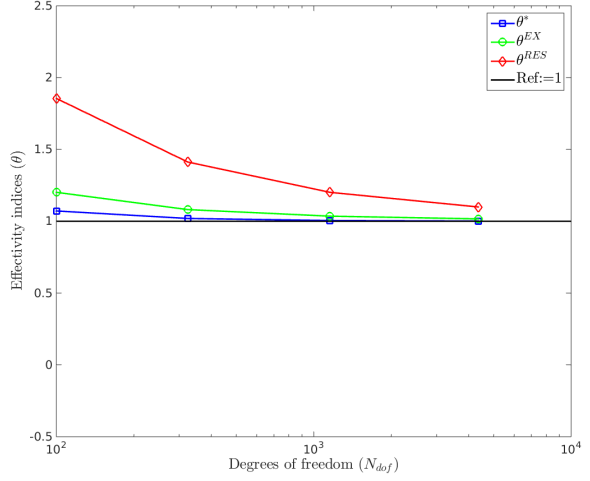
From the error plots it can be noticed that the exact error in the higher order approximation $\|u - u_h^*\|_{RE}$ converges with the rate of one order higher than the exact error in original approximation $\|u - u_h\|_{RE}$.

The effectivity index comparison plots show that η_h^* provides a more accurate estimation of the exact error than the exact estimate η_h^{EX} and residual based estimate η_h^{RES} for all presented cases. The estimate η_h^{EX} presents the best error approximation one can achieve after applying the triangle inequality on the exact error when the exact solution u is available. For the considered example we also noticed that the estimators η_h^* and η_h^{EX} are asymptotically exact on refined meshes while the residual based estimator η_h^{RES} also shows a very good approximation of the exact error on refined meshes. The effectivity index for η_h^* are within the range of [1, 1.2].

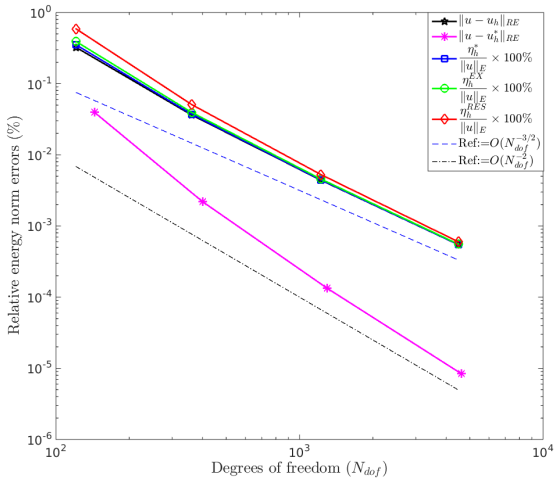
In Figure 7 we numerically illustrate that the saturation property given in Equation (42) holds for k -refined approximations. In fact for the present case with smooth exact solution we obtain that $C_{sat} = O(h)$ —a much stronger behavior than that is required for the saturation assumption.



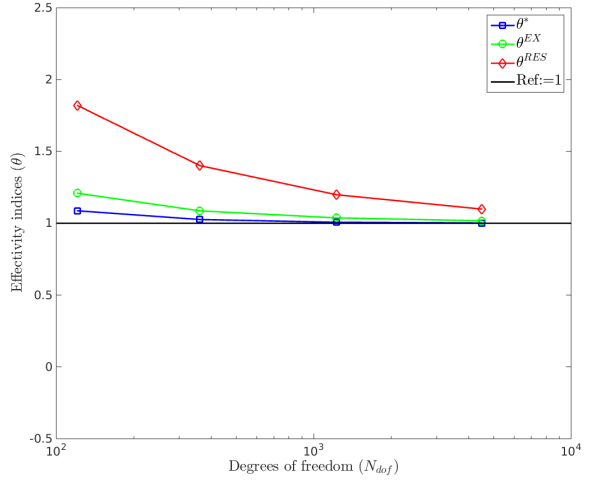
(a) Error plots, $V_h := \mathcal{S}_h^{2,1}$, $V_h^* = \mathcal{S}_h^{3,2}$



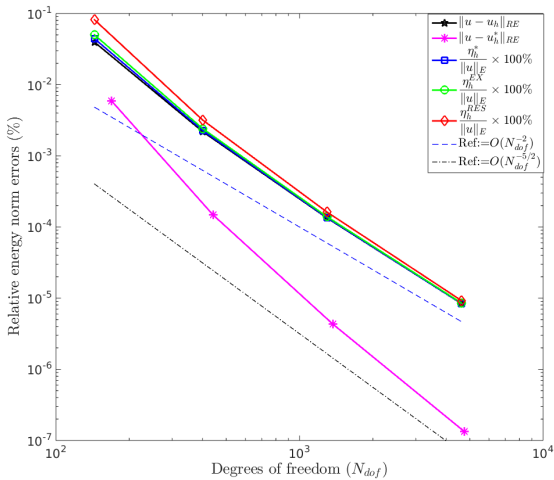
(b) Effectivity index θ



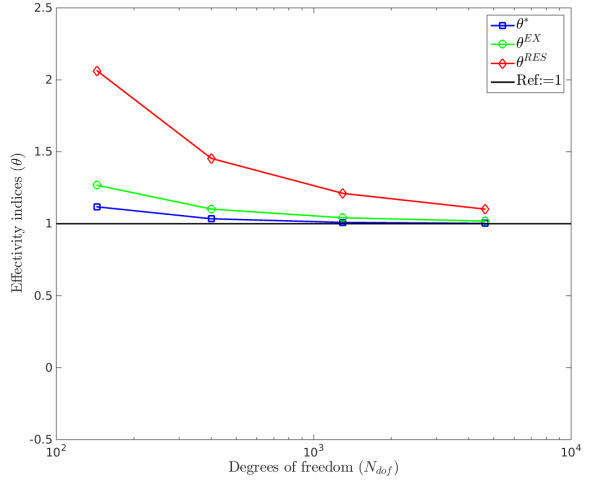
(c) Error plots, $V_h := \mathcal{S}_h^{3,2}$, $V_h^* = \mathcal{S}_h^{4,3}$



(d) Effectivity index θ

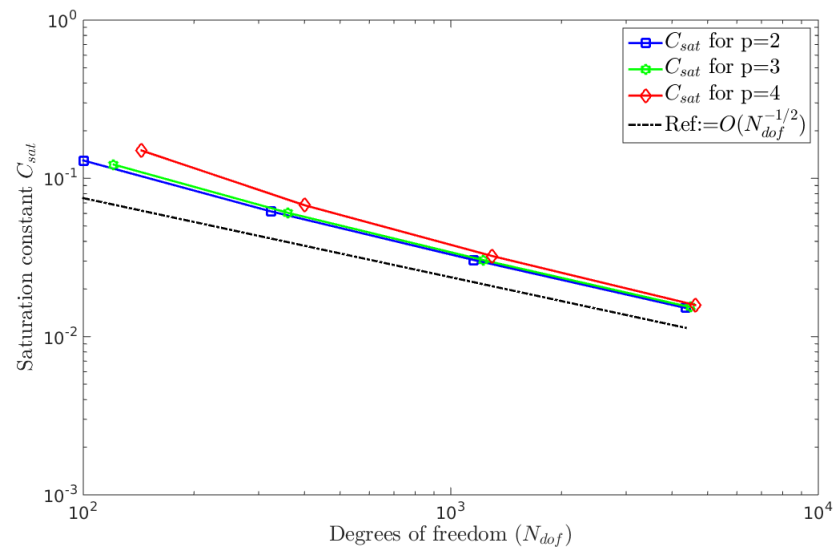


(e) Error plots, $V_h := \mathcal{S}_h^{4,3}$, $V_h^* = \mathcal{S}_h^{5,4}$



(f) Effectivity index θ

Figure 6: **Sinus problem:** Plots of relative errors (%) in energy norm and effectivity index $\theta^{(\cdot)}$, $\cdot = \{\ast, RES, EX\}$ obtained using $V_h := \mathcal{S}_h^{p,p-1}$ and $V_h^* := \mathcal{S}_h^{p+1,p}$ for $p = 2, 3, 4$ (respectively in each row) with uniform h -refinements.



(a) C_{sat} for Example 1

Figure 7: **Sinus problem:** Plots of Saturation constant C_{sat} obtained with uniform h -refinements and degrees $p = 2, 3, 4$.

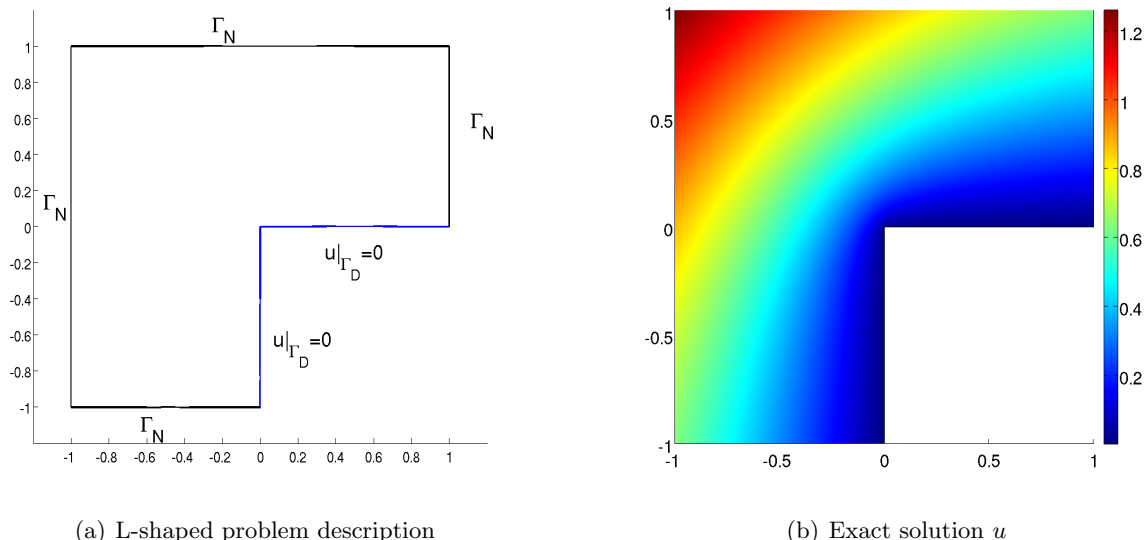


Figure 8: **L-shaped problem:** Problem description and Exact solution u .

6.4. Adaptive refinement results

Example 2. (L-shaped domain problem)

The governing equation of the L-shaped domain problem is

$$\Delta u = 0 \quad \text{in } \Omega, \quad (58)$$

with the boundary conditions

$$u = 0 \quad \text{on } \Gamma_D \quad \text{and} \quad \frac{\partial u}{\partial n} = g \quad \text{on } \Gamma_N, \quad (59)$$

Here $\Omega = (-1, 1)^2 \setminus (0, 1) \times (-1, 0)$ is a L-shaped domain and g is constructed to correspond to the exact solution

$$u(x, y) = r^{\frac{2}{3}} \sin\left(\frac{2\theta}{3}\right), \quad \text{with } r = (x^2 + y^2)^{\frac{1}{2}}, \quad \theta = \tan^{-1}\left(\frac{y}{x}\right). \quad (60)$$

The set up of the problem with given boundary conditions and the exact solution u are shown in Figure 8.

For the given elliptic problem, the re-entrant corner at $(0, 0)$ in the domain cause a singularity in the solution. It is known that the convergence for uniform mesh refinement is limited by the strength of the singularity, i.e. the convergence rate (versus degrees of freedoms) is equal to $-1/3$. For problems where the solution is not sufficiently smooth, $u \notin H^{p+1}(\Omega)$, as is the case for the L-shaped domain problem, we do not obtain optimal convergence rate when we do uniform mesh refinement. In particular, the use of high order polynomials is then inefficient.

The L-shaped domain geometry is modeled with two patches which join merely continuously $C^0, k = 0$ along the line segment from $(0, 0)$ to $(-1, 1)$. Here the geometry parametrization does not quite fit into the framework of the single-patch spaces $\mathcal{S}_h^{p,k}(\mathcal{M})$, while we will show numerically that we obtained good results in this case. Similar to two patches considered in L-shaped domain geometry model one can also consider a simple three patches model by subdividing the L-shaped region into three congruent squares; parametrization would then not even be necessary. The L-shaped domain problem is solved using the linear, quadratic and cubic LR B-spline spaces $V_h : \mathcal{S}_h^{p,p-1}$, $p = 1, 2, 3$ with uniform h -refinements and adaptive h -refinements based on a posteriori error estimators η_h^{RES} and η_h^* . The error plots for the relative error (%) in energy norm and effectivity index for $\theta^{(\cdot)}, \cdot = \{*, RES, EX\}$, and the saturation constant using the approximation spaces $V_h := \mathcal{S}_h^{p,p-1}$ and k -refined spaces $V_h^* := \mathcal{S}_h^{p+1,p}$ for $p = 1, 2, 3$ with uniform and adaptive h -refinement are shown in Figures 9-11. The numerical results of uniform and adaptive h -refinement using the error estimators η_h^{RES} and η_h^* are shown in left and right column of Figures 9-11, respectively.

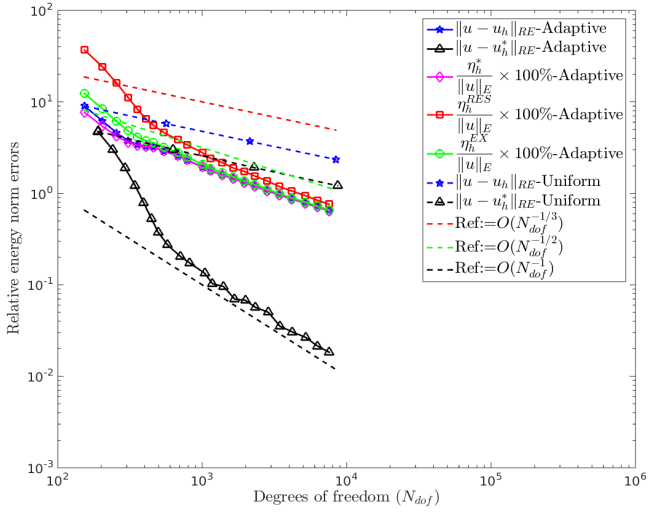
From the error plots presented in first row of Figures 9-11 the difference in the convergence rate of exact errors obtained by means of uniform h -refinement and adaptive h -refinement is clearly noticed. For uniform h -refinements the exact energy error for u_h converges at the rate of $O(N_{dof}^{-1/3})$ for all approximation spaces, this is clearly caused by the singularity present in the problem. While in the case of adaptive refinement we achieve an optimal rate of convergence for all the cases presented here with both error estimators. It can also be noticed that the exact error in higher order approximation $\|u - u_h^*\|_{RE}$ converges asymptotically with one order higher rate than the exact error in original approximation $\|u - u_h\|_{RE}$.

The effectivity index comparison plots with uniform h -refinement and adaptive refinement clearly show that η_h^* provides more accurate estimation of the exact error than the residual based estimate η_h^{RES} for all cases. The estimate η_h^{EX} presents here the best error approximation one can achieve after applying the triangle inequality and is computable only when the analytical solution u is known. For the L-shaped domain problem we also noticed that the estimators η_h^* and η_h^{EX} are asymptotically exact on refined meshes. Furthermore, the residual based estimator η_h^{RES} also shows a very good approximation of the exact error on adaptive refined meshes and we also have asymptotically convergence for the corresponding effectivity index. Since the present residual based estimator η_h^{RES} involves the residual of a high order approximation u_h^* its behavior is different than the standard residual estimator based on u_h . The error estimator η_h^{RES} is very conservative on coarse meshes and then converges to the exact error when proper adaptive mesh refinement has been achieved for the higher order approximation u_h^* . On coarse meshes the residual term involved in the estimator η_h^{RES} provides a safeguard in the error estimation process as the estimator η_h^* in these

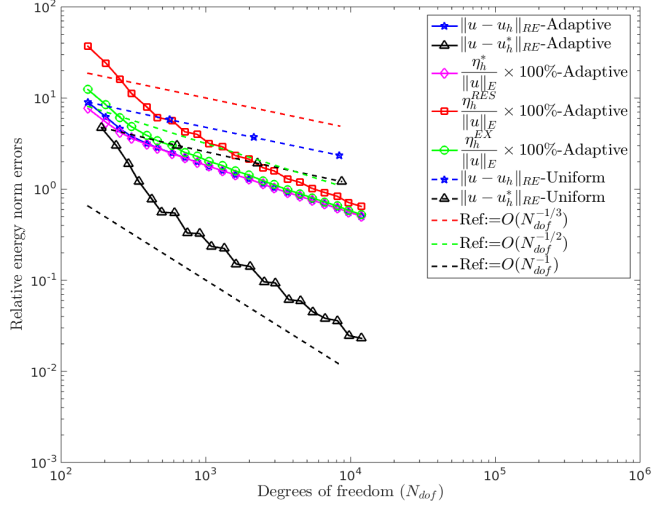
cases generally underestimates the error. When we compare the exact error in u^h we notice that the results provided by using the estimator η_h^{RES} to drive the adaptive refinement are slightly better than the results obtained with use of the η_h^* estimator.

In third row of Figures 9-11 we numerically illustrate that the saturation property given in Equation (42) holds for k -refined approximations even on non-smooth solution case on coarse meshes. In fact, for all the cases, asymptotically we obtain that $C_{sat} = O(h)$ —a much stronger behavior than that is required for the saturation assumption. We also noticed that the value of saturation constant C_{sat} with the application of error estimator η_h^{RES} decrease more rapidly in comparison to the case with the error estimator η_h^* . Thus we can obtain a more accurate approximation u_h^* with estimator η_h^{RES} than with the use of η_h^* .

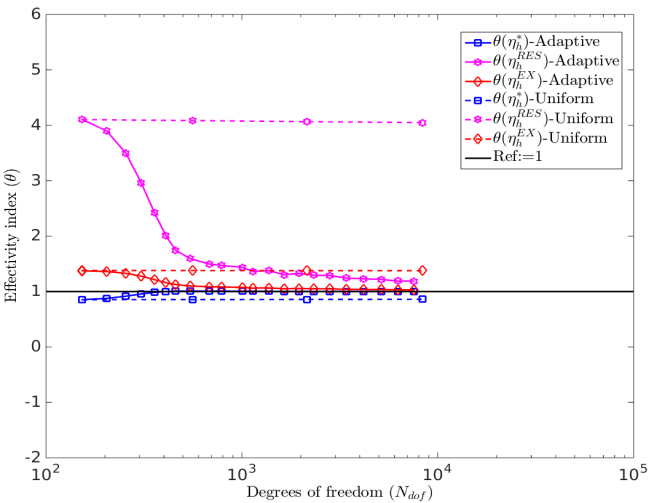
The comparison of root mean square of the exact element error given in Equation (48) which measures the deviation from an uniform element error distribution are shown in Figure 12. For the uniform h -refinement case we observed that the root mean square error will not converges because of pollution error present in the L-shaped problem while the adaptive refinement procedure provides a sequence of meshes that seems to satisfy $\lim_{h \rightarrow 0} \|e\|_{RMS} = 0$. The adaptive LR-meshes at step 20 for all the different cases are also displayed in Figure 13.



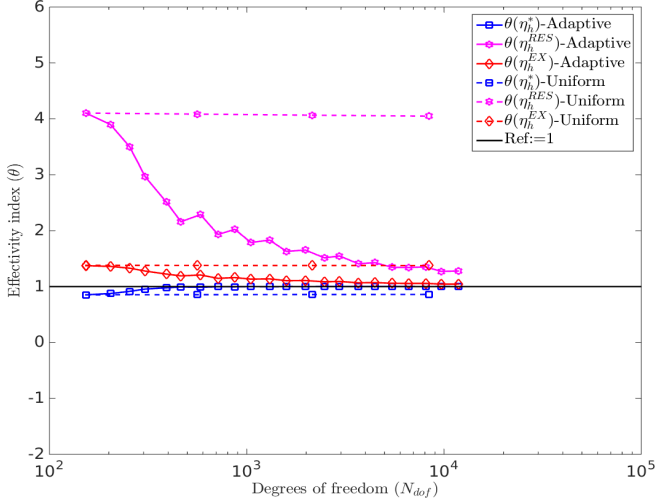
(a) Relative errors (%) in energy norm plots



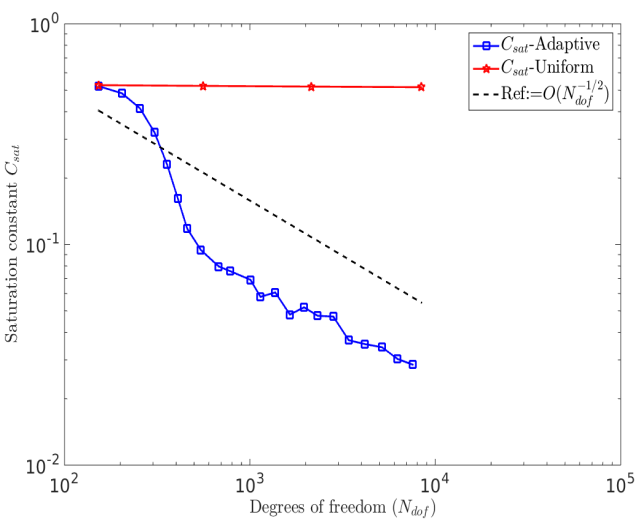
(b) Relative errors (%) in energy norm plots



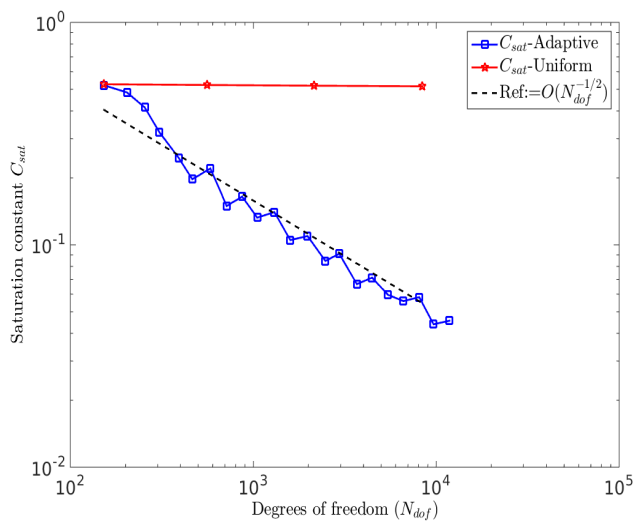
(c) Effectivity index θ



(d) Effectivity index θ

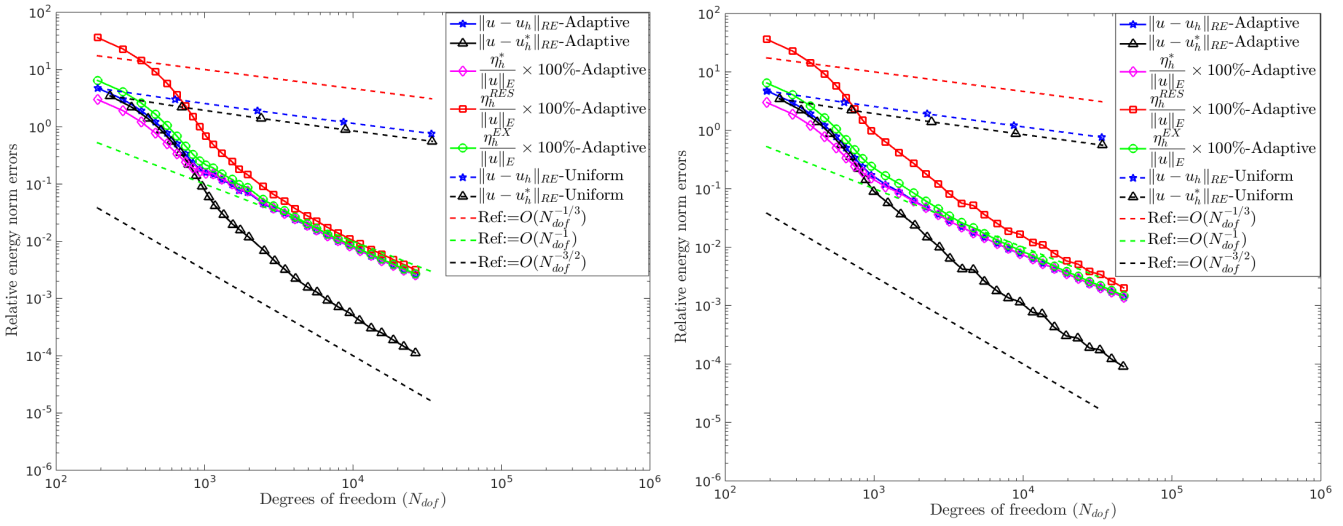


(e) Saturation constant C_{sat}



(f) Saturation constant C_{sat}

Figure 9: **L-shaped domain problem:** Case $V_h = \mathcal{S}^{1,0}(\mathcal{M})$ and $V_h^* = \mathcal{S}^{2,1}(\mathcal{M})$. Plots of relative errors (%) in energy norm, effectivity index θ and saturation constant C_{sat} obtained using η_h^{RES} (at left) and η_h^* (at right) error estimators in adaptive isogeometric analysis with LR B-splines.



(a) Relative errors (%) in energy norm plots

(b) Relative errors (%) in energy norm plots

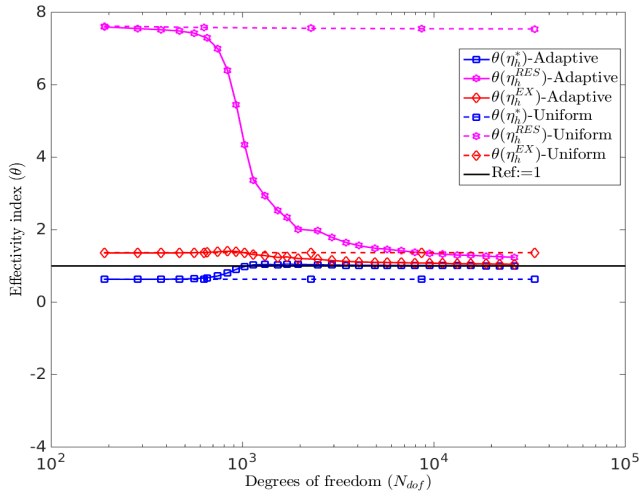
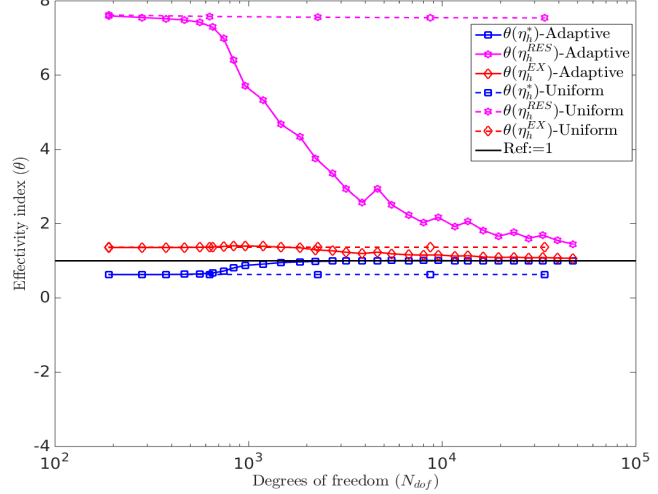
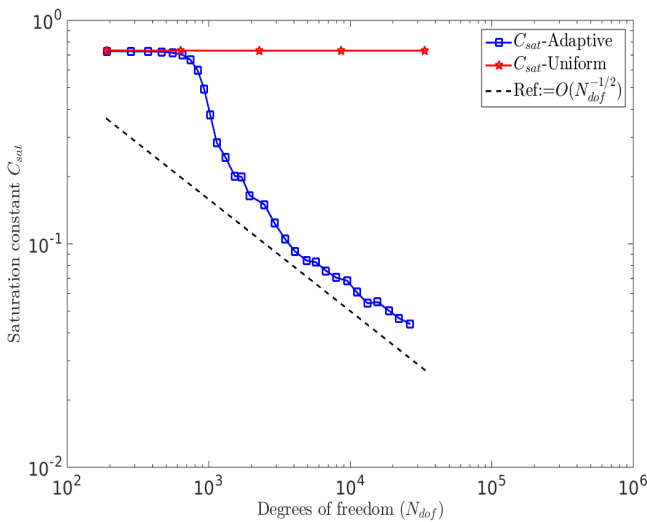
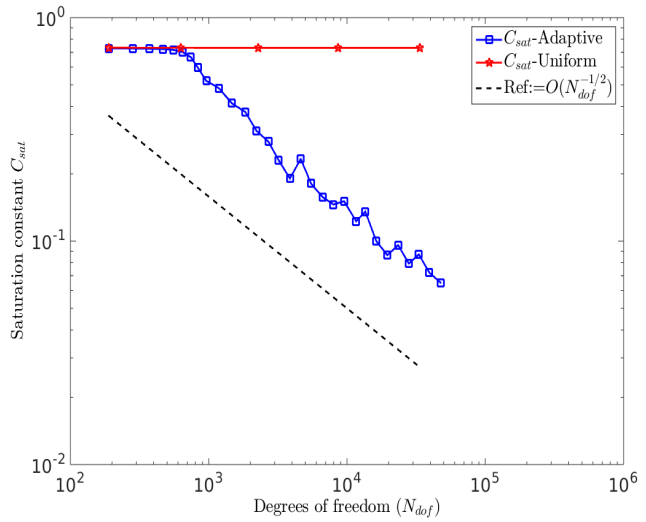
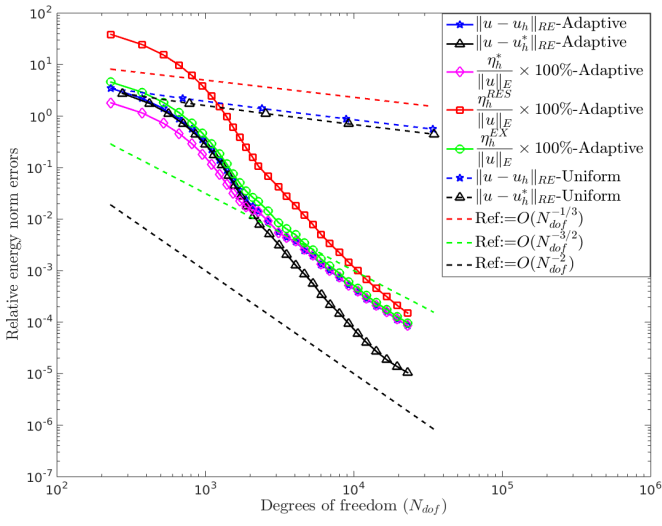
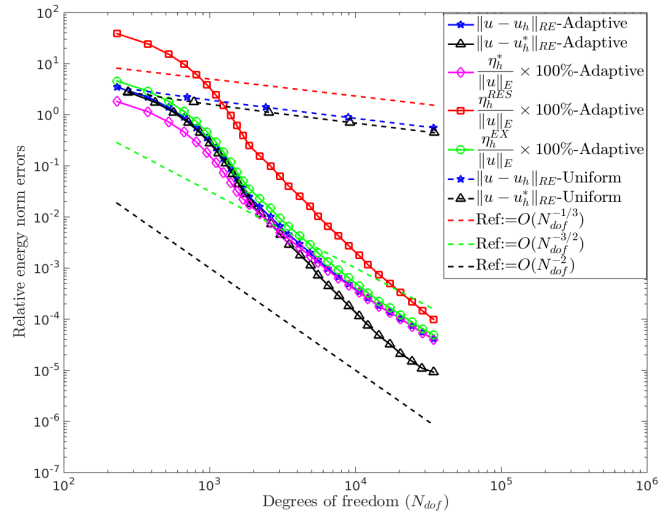
(c) Effectivity index θ (d) Effectivity index θ (e) Saturation constant C_{sat} (f) Saturation constant C_{sat}

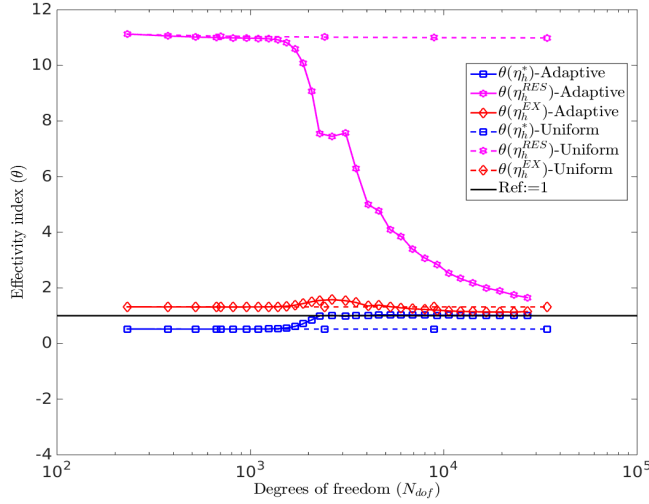
Figure 10: **L-shaped domain problem:** Case $V_h = \mathcal{S}^{2,1}(\mathcal{M})$ and $V_h^* = \mathcal{S}^{3,2}(\mathcal{M})$. Plots of relative errors (%) in energy norm, effectivity index θ and saturation constant C_{sat} obtained using η_h^{RES} (at left) and η_h^* (at right) error estimators in adaptive isogeometric analysis with LR B-splines.



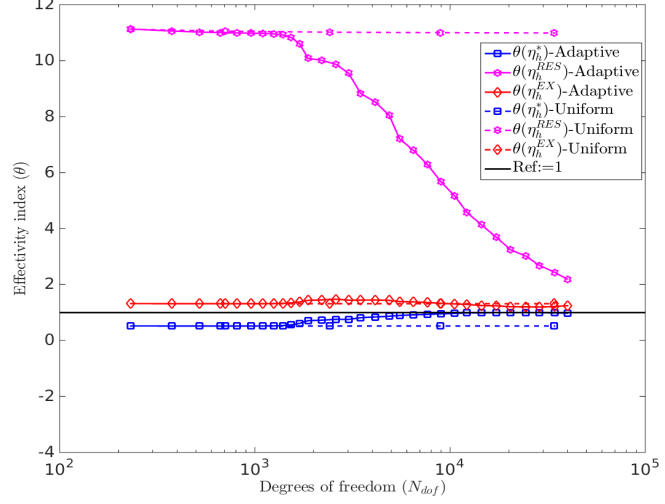
(a) Relative errors (%) in energy norm plots



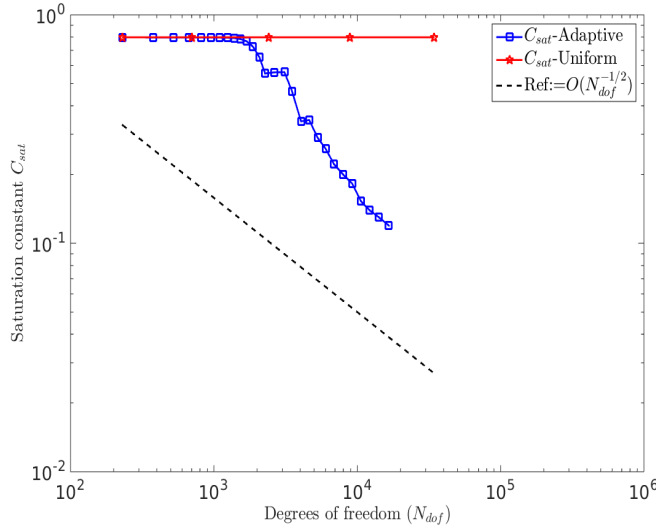
(b) Relative errors (%) in energy norm plots



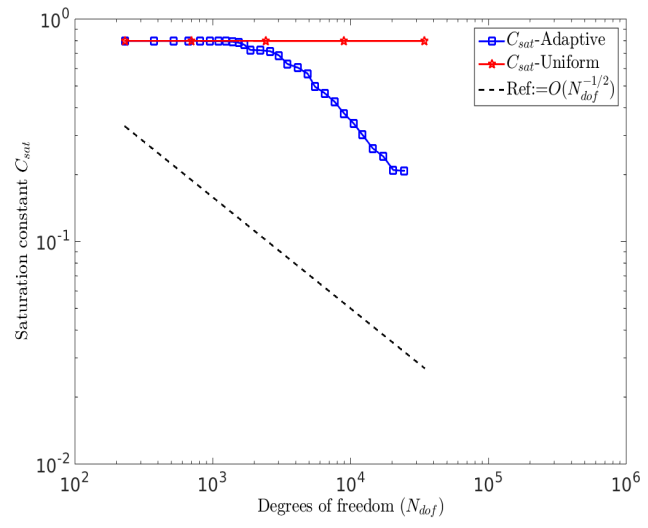
(c) Effectivity index θ



(d) Effectivity index θ

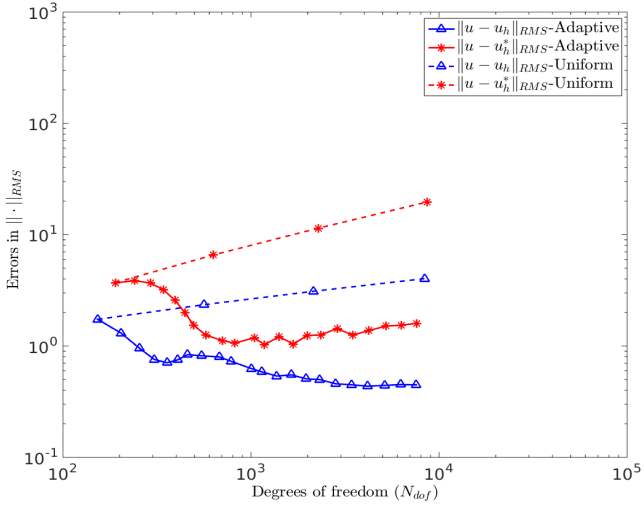


(e) Saturation constant C_{sat}

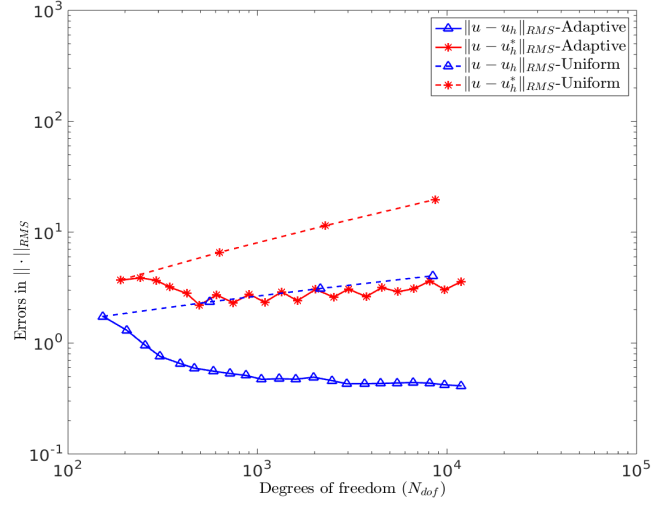


(f) Saturation constant C_{sat}

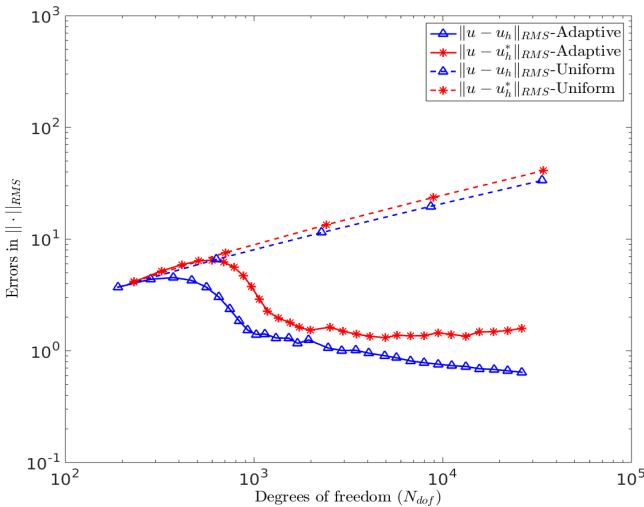
Figure 11: **L-shaped domain problem:** Case $V_h = \mathcal{S}^{3,2}(\mathcal{M})$ and $V_h^* = \mathcal{S}^{4,3}(\mathcal{M})$. Plots of relative errors (%) in energy norm, effectivity index θ and saturation constant C_{sat} obtained using η_h^{RES} (at left) and η_h^* (at right) error estimators in adaptive isogeometric analysis with LR B-splines.



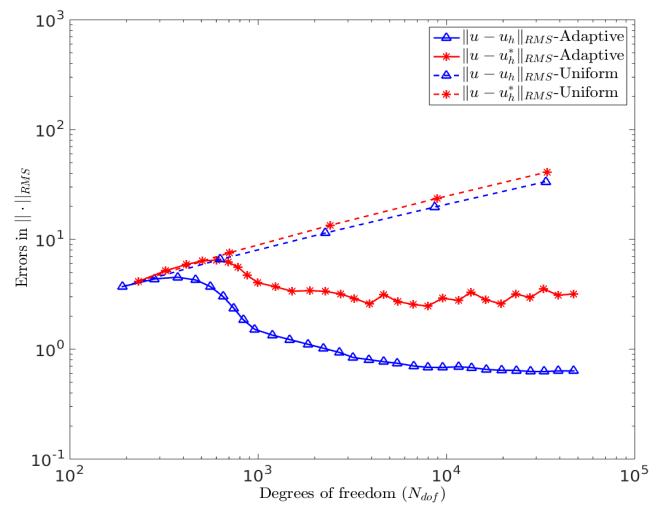
(a) $p = 1, k = 0$, Errors in $\|\cdot\|_{RMS}$ norm



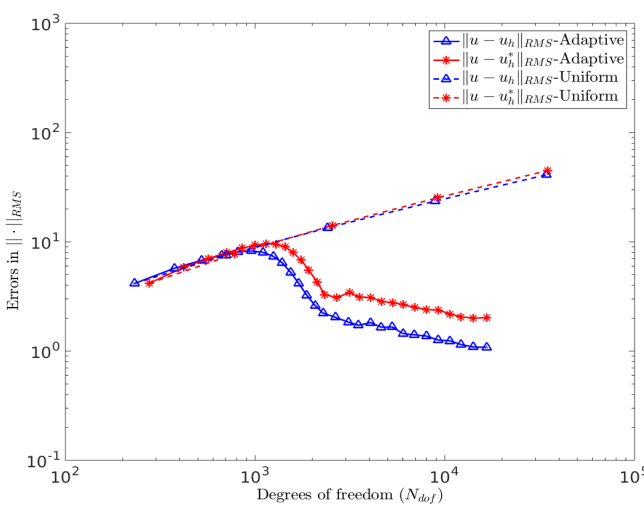
(b) $p = 1, k = 0$, Errors in $\|\cdot\|_{RMS}$ norm



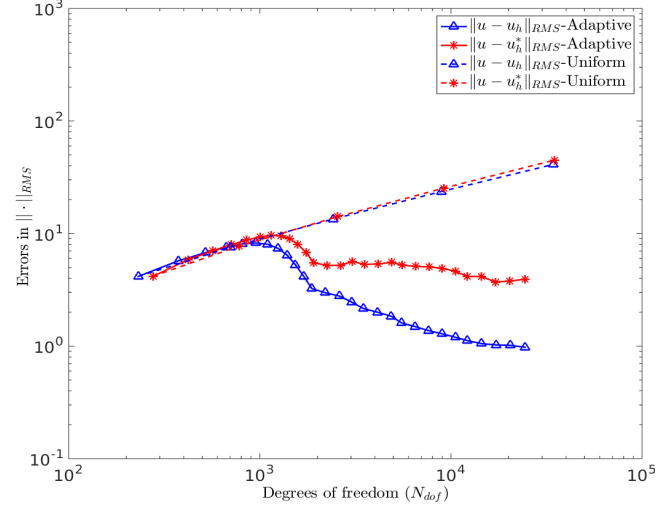
(c) $p = 2, k = 1$, Errors in $\|\cdot\|_{RMS}$ norm



(d) $p = 2, k = 1$, Errors in $\|\cdot\|_{RMS}$ norm

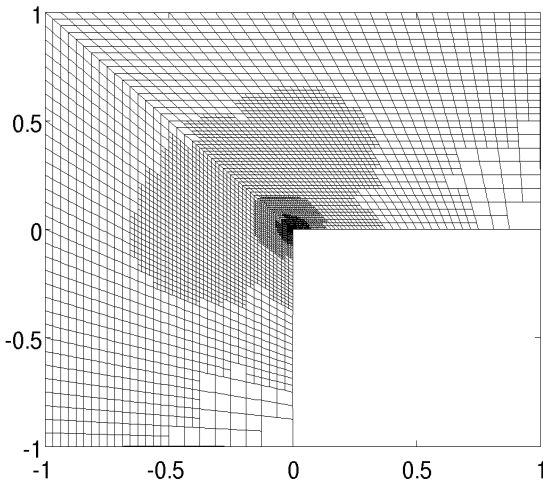


(e) $p = 3, k = 2$, Errors in $\|\cdot\|_{RMS}$ norm

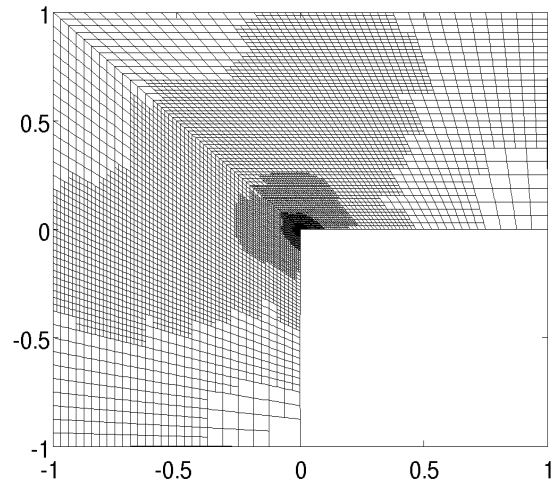


(f) $p = 3, k = 2$, Errors in $\|\cdot\|_{RMS}$ norm

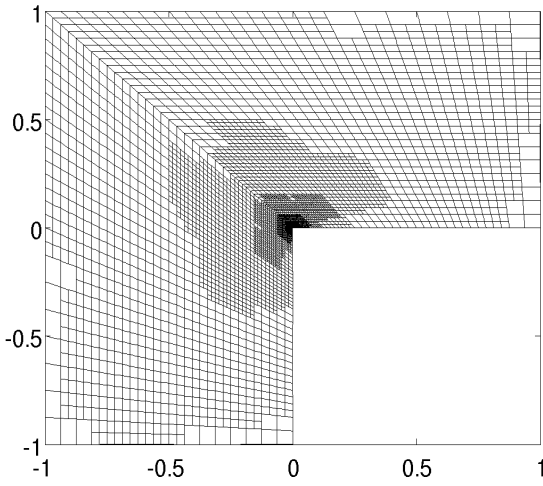
Figure 12: **L-shaped domain problem:** Plots of root mean square errors $\|\cdot\|_{RMS}$ obtained using $\mathcal{S}^{p,k}(\mathcal{M})-\mathcal{S}^{p+1,k+1}(\mathcal{M})$ based error estimators in adaptive isogeometric analysis with LR B-splines: η_h^{RES} (left) and η_h^* (right).



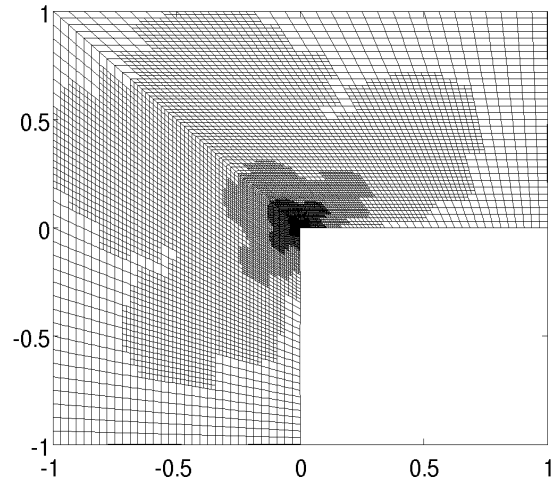
(a) $p = 1, k = 0, N_{dof} = 6257, N_{dof}^* = 6294$



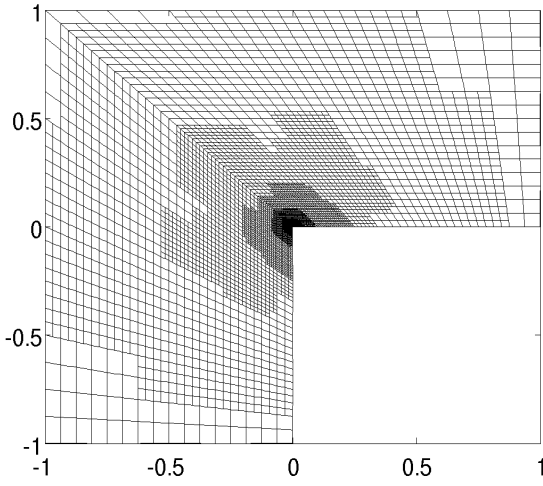
(b) $p = 1, k = 0, N_{dof} = 8075, N_{dof}^* = 8122$



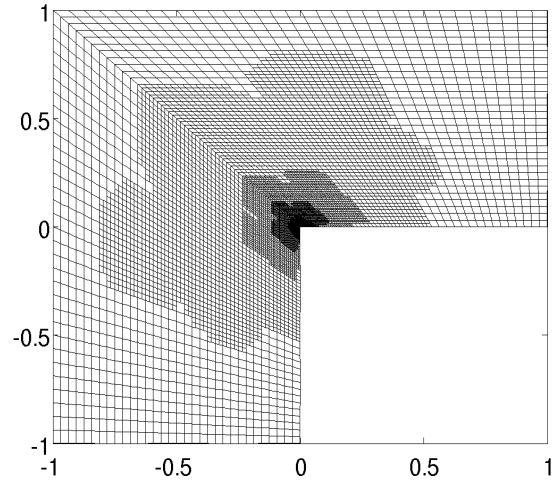
(c) $p = 2, k = 1, N_{dof} = 6017, N_{dof}^* = 6046$



(d) $p = 2, k = 1, N_{dof} = 7804, N_{dof}^* = 7892$



(e) $p = 3, k = 2, N_{dof} = 5694, N_{dof}^* = 5724$



(f) $p = 3, k = 2, N_{dof} = 7655, N_{dof}^* = 7681$

Figure 13: **L-shaped domain problem:** LR meshes obtained at intermediate refinement step 20 using $\mathcal{S}_h^{p,k}(\mathcal{M})$ - $\mathcal{S}_h^{p+1,k+1}(\mathcal{M})$ based error estimators in adaptive isogeometric analysis with LR B-splines: η_h^{RES} (left) and η_h^* (right). Here N_{dof} and N_{dof}^* represents degrees of freedom for $V_h = \mathcal{S}_h^{p,k}(\mathcal{M})$ and $V_h^* = \mathcal{S}_h^{p+1,k+1}(\mathcal{M})$ spaces, respectively.

6.5. A cost efficient approach

As we have discussed in Section 2 the cost to obtain a higher order approximation u_h^* using k -refined spaces will be almost twice to the original approximation u_h itself when full Gauss-quadrature points are used in the assembly procedure. Although the cost can be reduced by choosing the recently available selective and reduced integration rules in isogeometric analysis. But in this section, we present a different approach to reduce this cost which is based on reducing the number of degrees of freedom for u_h^* by coarsening the mesh by a factor of m in each direction. We remedy the reduction in accuracy that occurs due to mesh coarsening by increasing the polynomial degree by the same factor m . For this we define

$$V_h := \mathcal{S}_h^{p,k} \quad \text{and} \quad V_{mh}^* := \mathcal{S}_{mh}^{p+m,k+m}, \quad m = 1, 2, 4,$$

where V_{mh}^* represents a coarse and high order k -refined space of V_h at level m . For $m = 1$ we obtain the classical k -refined space as discussed in Section 2 and 4.

The assembly and solving cost ratio to obtain a higher order approximation u_h^* , similar to as presented in Table 2, using these new coarser and higher order k -refined spaces for $V_h := \mathcal{S}_h^{2,1}$ are shown in Table 6. This alternative *modified k-refinement* approach to obtain Serendipity pairings in isogeometric analysis is clearly a cost efficient approach where we may reduce the the cost ratio to less than 0.5.

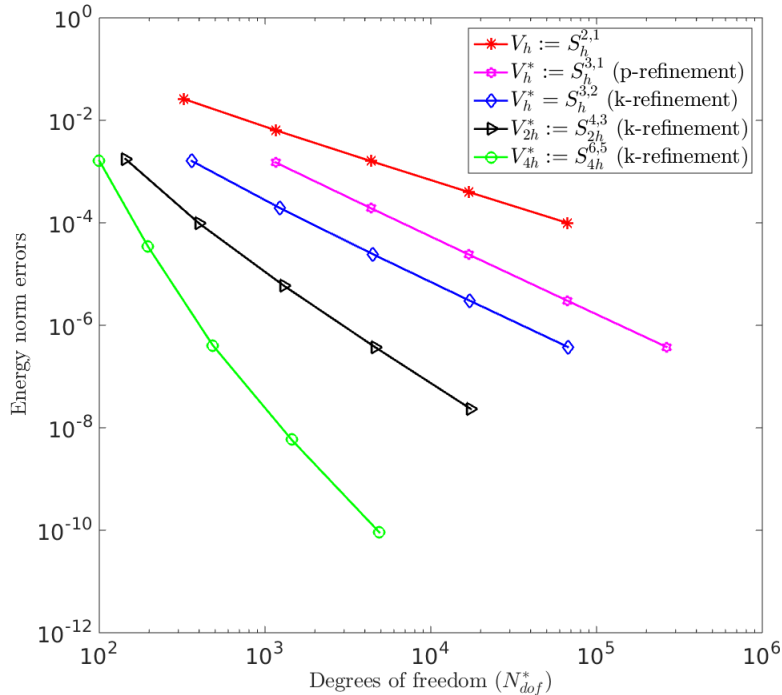
In Figure 14, energy error plots with uniform h -refinements of $V_h := \mathcal{S}_h^{2,1}$ and its modified k -refined spaces for the Sinus problem (Example 1) are given. The better accuracy per degrees of freedom achieved with these modified k -refined spaces are clearly visible.

Table 6: **Sinus problem:**Degrees of freedoms and timing for solving the Sinus problem using $V_h = \mathcal{S}_h^{2,1}(\mathcal{M})$ with different modified k -refined spaces V_h^* .

$V_h = \mathcal{S}_h^{2,1}(\mathcal{M})$ and $V_{2h}^* = \mathcal{S}_{2h}^{4,3}(\tilde{\mathcal{M}})$						
Mesh size	Degrees of freedom			Assembling time	Solving time	Total
	$N_{dof} = \dim(V_h)$	$N_{dof}^* = \dim(V_{2h}^*)$	$\frac{N_{dof}^*}{N_{dof}}$	$\frac{FE(u_h^*)}{FE(u_h)}$	$\frac{FE(u_h^*)}{FE(u_h)}$	$\frac{FE(u_h^*)}{FE(u_h)}$
8×8	100	64	0.64	0.63	0.66	0.63
16×16	324	144	0.44	0.64	0.10	0.63
32×32	1156	400	0.34	0.67	0.52	0.67
64×64	4356	1296	0.29	0.68	0.51	0.68
128×128	16900	4624	0.27	0.70	0.47	0.69

$V_h = \mathcal{S}_h^{2,1}(\mathcal{M})$ and $V_{4h}^* = \mathcal{S}_{4h}^{6,5}(\tilde{\mathcal{M}})$						
Mesh size	Degrees of freedom			Assembling time	Solving time	Total
	$N_{dof} = \dim(V_h)$	$N_{dof}^* = \dim(V_{4h}^*)$	$\frac{N_{dof}^*}{N_{dof}}$	$\frac{FE(u_h^*)}{FE(u_h)}$	$\frac{FE(u_h^*)}{FE(u_h)}$	$\frac{FE(u_h^*)}{FE(u_h)}$
8×8	100	64	0.64	0.50	0.92	0.51
16×16	324	100	0.31	0.44	0.08	0.44
32×32	1156	196	0.17	0.47	0.06	0.48
64×64	4356	484	0.11	0.49	0.04	0.49
128×128	16900	1444	0.09	0.51	0.19	0.50

The error plots for the comparison of relative error (%) in energy norm and effectivity indeces $\theta^{(\cdot)}$, $\cdot = \{*, RES, EX\}$ using the approximation spaces $V_h := \mathcal{S}_h^{2,1}$ and modified k -refined spaces $V_{mh}^* := \mathcal{S}_{mh}^{2+m,1+m}$ for $m = 2, 4$ (respectively in each row) with uniform h -refinements for the Sinus problem are shown in Figure 15. Here we consider a very



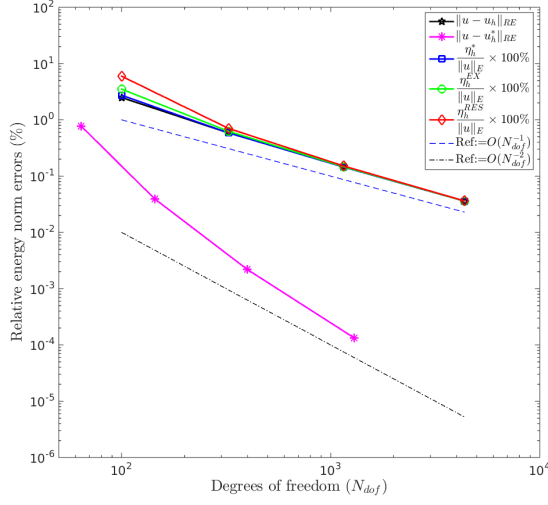
(a) Energy errors for $V_h := \mathcal{S}_h^{2,1}$

Figure 14: Energy errors with uniform h -refinements of $V_h := \mathcal{S}_h^{2,1}$ and its k -refined coarse spaces for Example 1.

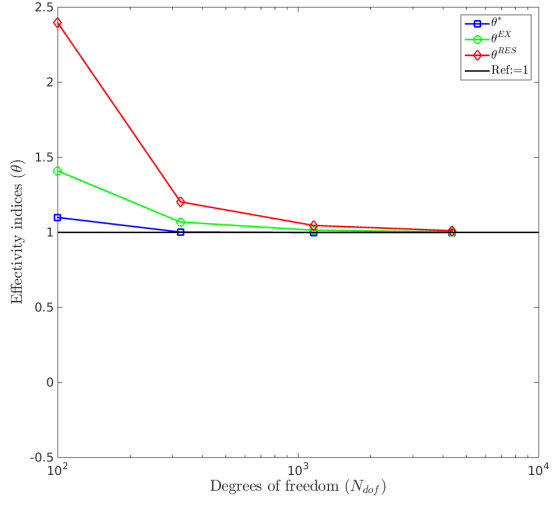
coarse starting mesh of (8×8) elements for the space $V_h := \mathcal{S}_h^{2,1}$ and the element mesh of (4×4) and (2×2) for V_{2h}^* and V_{4h}^* , respectively.

From the error plots it can be noticed that the exact error in the higher order approximation $\|u - u_h^*\|_{RE}$ obtained with modified k -refined spaces $V_h^* := \mathcal{S}_{mh}^{2+m,1+m}$ for $m = 2, 4$ converges with the rate $m + 2$ that is m order higher than the exact error in the original approximation $\|u - u_h\|_{RE}$. The high order convergence rates obtained with the modified k -refined spaces V_h^* improves the performance of all the herein proposed estimators. When we compare the error plots given in the first row of Figure 6 for $V_h := \mathcal{S}_h^{2,1}$ with the error plots of Figure 15 then a clear benefit of using modified k -refined spaces for V_{mh}^* can be noticed. We also notice that the performance of all the proposed error estimators are also improved in comparison to the case presented in first row of Figure 6. The estimators η_h^* and η_h^{EX} now becomes asymptotically exact on much coarser meshes while the residual based estimator η_h^{RES} , which was not asymptotically exact in Figure 6, now becomes asymptotically exact.

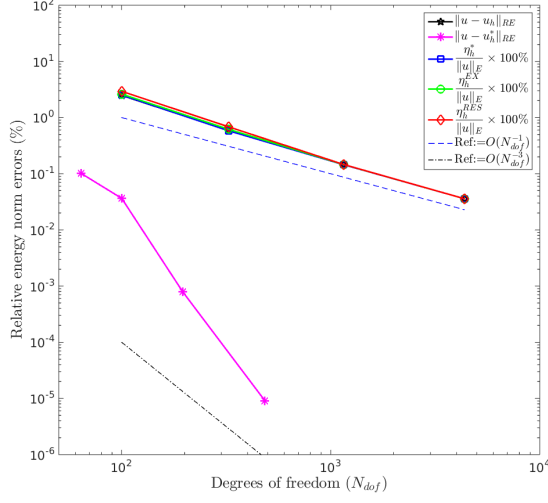
In Figure 16 we show that the saturation property given in Equation (42) holds for these modified k -refined approximations. For the present case with smooth exact solution we obtain that $C_{sat} = O(h^m)$ —a much stronger behavior than that is required for the saturation assumption.



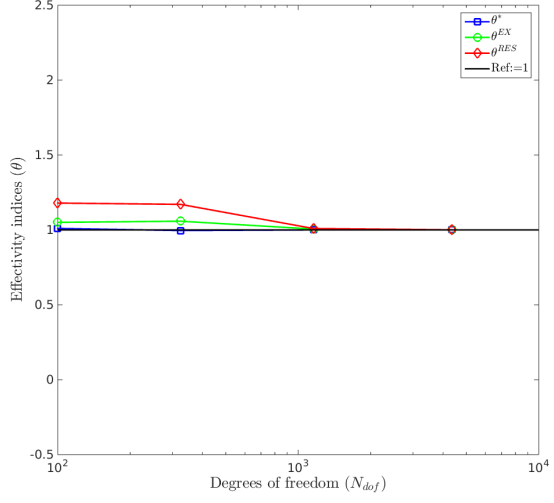
(a) Error plots, $V_h := \mathcal{S}_h^{2,1}$, $V_{2h}^* = \mathcal{S}_{2h}^{4,3}$



(b) Effectivity index θ

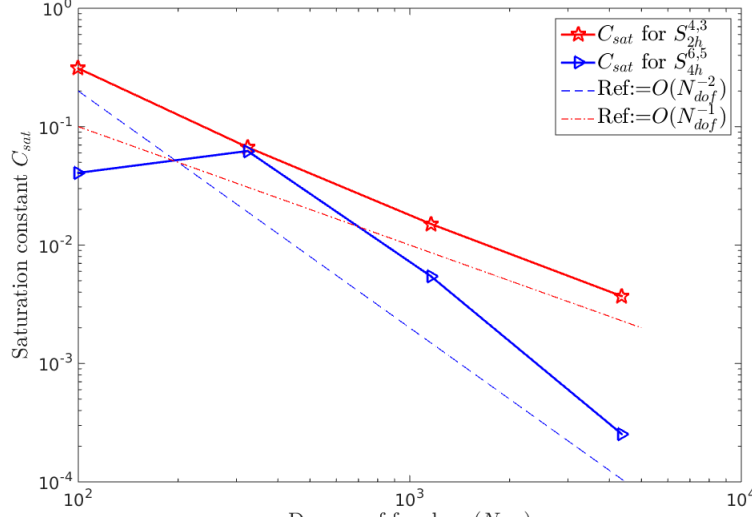


(c) Error plots, $V_h := \mathcal{S}_h^{2,1}$, $V_{4h}^* = \mathcal{S}_{4h}^{6,5}$



(d) Effectivity index θ

Figure 15: **Sinus problem:** Plots of relative errors (%) in energy norm and effectivity indeces $\theta^{(\cdot)}$, $\cdot = \{\ast, RES, EX\}$ obtained using $V_h := \mathcal{S}_h^{2,1}$ and $V_{mh}^* := \mathcal{S}_{mh}^{2+m,1+m}$ for $m = 2, 4$ (respectively in each row) with uniform h -refinements.



(a) C_{sat} for Example 1

Figure 16: Sinus problem: Plots of the Saturation constant C_{sat} obtained with uniform h -refinements and using $V_h := \mathcal{S}_h^{2,1}$ and the modified k -refined spaces $V_{mh}^* := \mathcal{S}_{mh}^{2+m,1+m}$ with $m = 2, 4$.

7. Conclusion and perspectives

The aim of the present study has been to propose a simple error estimation technique in adaptive isogeometric analysis. The main focus was to present a serendipity pairing of discrete approximation spaces $\mathcal{S}_h^{p,k}(\mathcal{M})-\mathcal{S}_h^{p+1,k+1}(\mathcal{M})$ using LR B-splines technology of [27]. Using this discrete pairing of spaces we propose two simple a posteriori error estimators η_h^* and η_h^{RES} for solving second order elliptic problems using adaptive isogeometric analysis. The main findings of the articles are:

- For smooth elliptic problems with uniform h -refinement we obtain:
 - A higher convergence rate for u^* compared to u^h
 - asymptotically exact error estimate for η_h^* on refined meshes
 - conservative error estimate with η_h^{RES}
- For non-smooth elliptic problems with adaptive h -refinement we obtain:
 - Optimal convergence rate, i.e. $O(h^p)$ for u^h measured in energy norm
 - a higher convergence rate for u^* compared to u^h
 - asymptotically exact error estimate for η_h^* on adaptive refined meshes
 - conservative error estimate with η_h^{RES}
 - asymptotically optimal element error distribution

Furthermore, we briefly report results obtained by an even more cost efficient approach where we consider a coarser mesh but higher order k -refined spaces $\mathcal{S}_{mh}^{p+m,k+m}$, $m = 1, 2, 4$. For the smooth problems with uniform h -refinement this approach seems to be very promising but to use it in adaptive isogeometric analysis a further study is needed.

In this article, we have discussed the general behavior of some different approaches using h -, p -, and k -refinement to refine a given discrete approximation space V_h into V_h^* in order to obtain a more accurate approximation u_h^* compared to u_h . Through the numerical study we clearly demonstrated the benefits of considering a discrete pair of approximation spaces $\mathcal{S}_h^{p,k}(\mathcal{M})-\mathcal{S}_h^{p+1,k+1}(\mathcal{M})$ obtained using k -refinement in solving the elliptic PDEs. Looking

forward we assume that computational costs related to assembly of coefficient matrices in isogeometric analysis will be significantly reduced, after some more research on selective integration rules, and this will make k -refinement even more efficient than p -refinement.

The authors are of the opinion that the approach presented herein is very suitable for a posteriori error estimation in isogeometric analysis. In particular we think it is especially suited for goal oriented error estimation. Recently, the authors in [31] considered a discrete pair of approximation spaces $S_h^{p,k}(\mathcal{M})$ - $S_h^{p+1,k}(\mathcal{M})$ obtained through p -refinement and using hierarchical B-splines for the goal oriented adaptive isogeometric analysis. In the near future, we will address goal oriented error estimation based on adaptive h -refinement using LR B-splines methodology ([27]) by considering the serendipity pairing of discrete approximation spaces $S_h^{p,k}(\mathcal{M})$ - $S_h^{p+1,k+1}(\mathcal{M})$ presented herein.

Acknowledgements

The authors acknowledge the financial support from the Norwegian Research Council and the industrial partners of the ICADA project (RCN grant no: 187993) (Ceetron, DNV GL and Statoil) and the FME NOWITECH (RCN grant no: 193823/S60) (www.nowitech.no). They also acknowledge the support from the other co-workers in the IFEM software team.

The authors gratefully acknowledge the valuable comments and suggestions from the anonymous referees.

References

- [1] C. Adam, T. J. R. Hughes, S. Bouadallahc, M. Zarrougd, and H. Maitournama. Selective and reduced numerical integrations for nurbs-based isogeometric analysis. *Comput. Methods Appl. Mech. Engrg.*, 284:732–761, 2015.
- [2] M. Ainsworth and J. T. Oden. *A posteriori error estimation in finite element analysis*. Pure and Applied Mathematics (New York). Wiley-Interscience [John Wiley & Sons], New York, 2000.
- [3] F. Auricchio, F. Calabro, T. J. R. Hughes, A. Reali, and G. Sangalli. A simple algorithm for obtaining nearly optimal quadrature rules for NURBS-based isogeometric analysis. *Comput. Methods Appl. Mech. Engrg.*, 249/252:15–27, 2012.
- [4] R. E. Bank. Hierarchical bases and the finite element method. In *Acta numerica, 1996*, volume 5 of *Acta Numer.*, pages 1–43. Cambridge Univ. Press, Cambridge, 1996.
- [5] R. E. Bank and R. K. Smith. A posteriori error estimates based on hierarchical bases. *SIAM J. Numer. Anal.*, 30(4):921–935, 1993.
- [6] R. E. Bank and A. Weiser. Some a posteriori error estimators for elliptic partial differential equations. *Math. Comp.*, 44(170):283–301, 1985.
- [7] Y. Bazilevs, L. Beirão da Veiga, J. A. Cottrell, T. J. R. Hughes, and G. Sangalli. Isogeometric analysis: approximation, stability and error estimates for h -refined meshes. *Math. Models Methods Appl. Sci.*, 16(7):1031–1090, 2006.
- [8] Y. Bazilevs, V. M. Calo, J. A. Cottrell, J. A. Evans, T. J. R. Hughes, S. Lipton, M. A. Scott, and T. W. Sederberg. Isogeometric analysis using T-splines. *Comput. Methods Appl. Mech. Engrg.*, 199(5-8):229–263, 2010.
- [9] L. Beirão da Veiga, A. Buffa, J. Rivas, and G. Sangalli. Some estimates for h - p - k -refinement in isogeometric analysis. *Numer. Math.*, 118(2):271–305, 2011.
- [10] L. Beirão da Veiga, A. Buffa, G. Sangalli, and R. Vázquez. Mathematical analysis of variational isogeometric methods. *Acta Numerica*, 23:157–287, 5 2014.

- [11] L. Beirão da Veiga, D. Cho, and G. Sangalli. Anisotropic NURBS approximation in isogeometric analysis. *Comput. Methods Appl. Mech. Engrg.*, 209/212:1–11, 2012.
- [12] A. Bressan. Some properties of LR-splines. *Comput. Aided Geom. Design*, 30(8):778–794, 2013.
- [13] A. Buffa, D. Cho, and M. Kumar. Characterization of T-splines with reduced continuity order on T-meshes. *Comput. Methods Appl. Mech. Engrg.*, 201/204:112–126, 2012.
- [14] A. Buffa and C. Giannelli. Adaptive isogeometric methods with hierarchical splines: error estimator and convergence. *Preprint, arXiv:1502.00565*, 2015.
- [15] J. A. Cottrell, T. J. R. Hughes, and Y. Bazilevs. *Isogeometric Analysis. Toward Integration of CAD and FEA*. Pure and Applied Mathematics (New York). John Wiley & Sons, 2009.
- [16] T. Dokken, T. Lyche, and K. F. Pettersen. Polynomial splines over locally refined box-partitions. *Comput. Aided Geom. Design*, 30(3):331–356, 2013.
- [17] M. R. Dörfel, B. Jüttler, and B. Simeon. Adaptive isogeometric analysis by local h -refinement with T-splines. *Comput. Methods Appl. Mech. Engrg.*, 199(5-8):264–275, 2010.
- [18] S. Ferraz-Leite, C. Ortner, and D. Praetorius. Convergence of simple adaptive Galerkin schemes based on $h-h/2$ error estimators. *Numer. Math.*, 116(2):291–316, 2010.
- [19] D.R. Forsey and R.H. Bartels. Hierarchical b-spline refinement. *Comput. Graph.*, 22:205–212, 1998.
- [20] C. Giannelli, B. Jüttler, and H. Speleers. THB-splines: the truncated basis for hierarchical splines. *Comput. Aided Geom. Design*, 29(7):485–498, 2012.
- [21] E. Hairer, S. P. Nørsett, and G. Wanner. *Solving ordinary differential equations. I*, volume 8 of *Springer Series in Computational Mathematics*. Springer-Verlag, Berlin, 1987. Nonstiff problems.
- [22] M. Hillman, J. S. Chen, and Y. Bazilevs. Variationally consistent domain integration for isogeometric analysis. *Comput. Methods Appl. Mech. Engrg.*, 284:521–540, 2015.
- [23] K. Höllig. *Finite element methods with B-splines*, volume 26 of *Frontiers in Applied Mathematics*. Society for Industrial and Applied Mathematics (SIAM), Philadelphia, PA, 2003.
- [24] T. J. R. Hughes, J. A. Cottrell, and Y. Bazilevs. Isogeometric analysis: CAD, finite elements, NURBS, exact geometry and mesh refinement. *Comput. Methods Appl. Mech. Engrg.*, 194(39-41):4135–4195, 2005.
- [25] T. J. R. Hughes, A. Reali, and G. Sangalli. Efficient quadrature for NURBS-based isogeometric analysis. *Comput. Methods Appl. Mech. Engrg.*, 199:301–313, 2010.
- [26] K. A. Johannessen. *An adaptive isogeometric finite element analysis*. 2009. Master thesis, Norwegian University of Science and Technology, Norway.
- [27] K. A. Johannessen, T. Kvamsdal, and T. Dokken. Isogeometric analysis using LR B-splines. *Comput. Methods Appl. Mech. Engrg.*, 269:471–514, 2014.
- [28] S. K. Kleiss and S. Tomar. Guaranteed and sharp a posteriori error estimates in isogeometric analysis. *Preprint, arXiv:1304.7712*, 2013.
- [29] R. Kraft. *Adaptive and Linearly Independent Multilevel B-splines*. Bericht. SFB 404, Geschäftsstelle, 1997.
- [30] M. Kumar, T. Kvamsdal, and K. A. Johannessen. Superconvergent patch recovery and a posteriori error estimation technique in adaptive isogeometric analysis. *Comput. Methods Appl. Mech. Engrg.*, Submitted, 2014.
- [31] G. Kuru, C. V. Verhoosel, K. G. van der Zee, and E. H. van Brummelen. Goal-adaptive isogeometric analysis with hierarchical splines. *Comput. Methods Appl. Mech. Engrg.*, 270:270–292, 2014.

- [32] S. I. Repin. A posteriori error estimates for approximate solutions to variational problems with strongly convex functionals. *J. Math. Sci. (New York)*, 97(4):4311–4328, 1999. Problems of mathematical physics and function theory.
- [33] S. I. Repin. A posteriori error estimation for variational problems with uniformly convex functionals. *Math. Comp.*, 69(230):481–500, 2000.
- [34] D. Schillinger, S. J. Hossain, and T. J. R. Hughes. Reduced Bézier element quadrature rules for quadratic and cubic splines in isogeometric analysis. *Comput. Methods Appl. Mech. Engrg.*, 277:1–45, 2014.
- [35] M. A. Scott, X. Li, T. W. Sederberg, and T. J. R. Hughes. Local refinement of analysis-suitable T-splines. *Comput. Methods Appl. Mech. Engrg.*, 213/216:206–222, 2012.
- [36] M. A. Scott, D. C. Thomas, and E. J. Evans. Isogeometric spline forests. *Comput. Methods Appl. Mech. Engrg.*, 269:222–264, 2014.
- [37] T. W. Sederberg, J. Zheng, A. Bakenov, and A. Nasri. T-splines and t-nurccs. *ACM Trans. Graph.*, 22(3):477–484, July 2003.
- [38] L. Tian, F. Chen, and Q. Du. Adaptive finite element methods for elliptic equations over hierarchical T-meshes. *J. Comput. Appl. Math.*, 236(5):878–891, 2011.
- [39] R. Verfürth. *A posteriori error estimation techniques for finite element methods*. Numerical Mathematics and Scientific Computation. Oxford University Press, Oxford, 2013.
- [40] A.-V. Vuong, C. Giannelli, B. Jüttler, and B. Simeon. A hierarchical approach to adaptive local refinement in isogeometric analysis. *Comput. Methods Appl. Mech. Engrg.*, 200(49-52):3554–3567, 2011.
- [41] P. Wang, J. Xu, J. Deng, and F. Chen. Adaptive isogeometric analysis using rational pht-splines. *Comput.-Aided Des.*, 43(11):1438–1448, 2011.
- [42] G. Xu, B. Mourrain, R. Duvigneau, and A. Galligo. Parameterization of computational domain in isogeometric analysis: methods and comparison. *Comput. Methods Appl. Mech. Engrg.*, 200(23-24):2021–2031, 2011.
- [43] G. Xu, B. Mourrain, R. Duvigneau, and A. Galligo. Optimal analysis-aware parameterization of computational domain in 3D isogeometric analysis. *Comput.-Aided Des.*, 45(4):812–821, 2013.
- [44] O. C. Zienkiewicz and J. Z. Zhu. A simple error estimator and adaptive procedure for practical engineering analysis. *Internat. J. Numer. Methods Engrg.*, 24(2):337–357, 1987.